Cell Reports
Medicine

Article

An epitope-directed mRNA vaccine inhibits tumor metastasis through the blockade of MICA/B α1/2 shedding

Graphical abstract

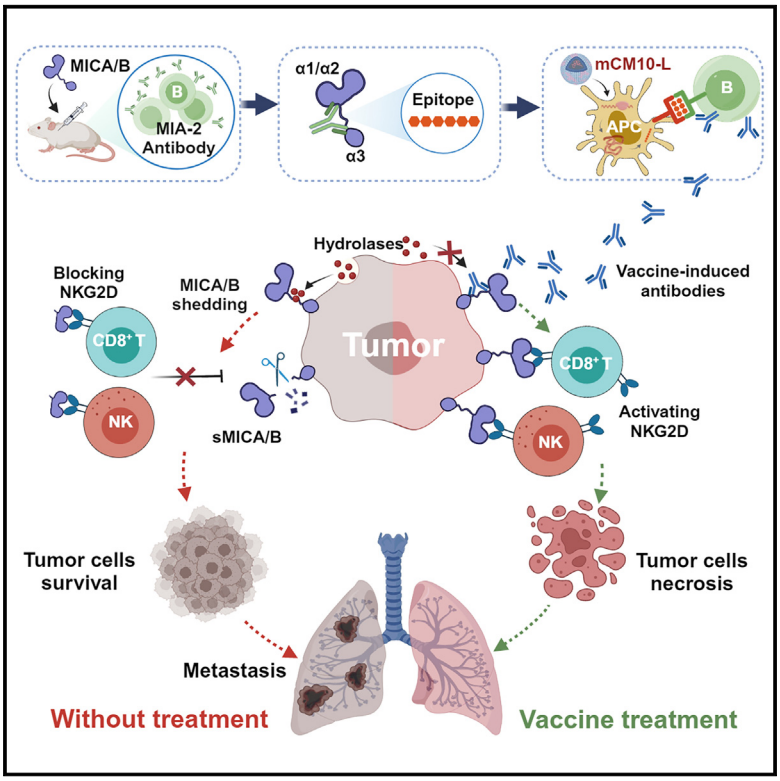

Highlights

- MICA/B α1/2 shedding associates with tumor metastasis in patients with colorectal cancer
- SHDTQQ is a linear B cell epitope in the MICA α3 proteolytic region
- Vaccines encoding the B cell epitope trigger a specific antimetastatic effect
- Interacting human organoid models can be used to evaluate B cell vaccines *in vitro*

Authors

Rui Wang, Jingni Wu, Yifeng Lin, ..., Shuyu Li, Caihua Wang, Yongliang Zhu

Correspondence

wangcaihua@zju.edu.cn (C.W.), ylzhu@zju.edu.cn (Y.Z.)

In brief

Wang et al. report an mRNA vaccine encoding a B cell epitope derived from the proteolytic region of MICA α3 and demonstrate that it exerts antimetastatic effect through activating B cell immunity to produce specific antibodies that block MICA/B α1/2 shedding in an *in-vitro*-interacting human organoid model and humanized mice.

Wang et al., 2025, Cell Reports Medicine 6, 101981
March 18, 2025
https://doi.org/10.1016/j.xcrm.2025.101981

CellPress

Cell Reports Medicine

CellPress
OPEN ACCESS

Article

An epitope-directed mRNA vaccine inhibits tumor metastasis through the blockade of MICA/B α1/2 shedding

Rui Wang,[1] Jingni Wu,[2] Yifeng Lin,[3] Yufei Xiao,[4] Bin Yang,[1] Sheng Yao,[5] Tianhui Pan,[3] Zhixuan Fu,[6] Shuyu Li,[1] Caihua Wang,[3,*] and Yongliang Zhu[1,7,*]

[1]Laboratory of Gastroenterology, Second Affiliated Hospital of Zhejiang University School of Medicine, Hangzhou, Zhejiang, China
[2]Department of International Healthcare Center and General Medicine, Second Affiliated Hospital of Zhejiang University School of Medicine, Hangzhou, Zhejiang, China
[3]Department of Gastroenterology, Second Affiliated Hospital of Zhejiang University School of Medicine, Hangzhou, Zhejiang, China
[4]Department of Clinical Laboratory, Second Affiliated Hospital of Zhejiang University School of Medicine, Hangzhou, Zhejiang, China
[5]Department of Hepatobiliary and Pancreatic Surgery, Second Affiliated Hospital of Zhejiang University School of Medicine, Hangzhou, Zhejiang, China
[6]Department of Colorectal Surgery, Zhejiang Cancer Hospital, Hangzhou, Zhejiang, China
[7]Lead contact
*Correspondence: wangcaihua@zju.edu.cn (C.W.), ylzhu@zju.edu.cn (Y.Z.)
https://doi.org/10.1016/j.xcrm.2025.101981

SUMMARY

Antigenic peptide-based mRNA vaccines have been explored for immunotherapeutic use in various types of cancer because of their advantages in activating durable and specific immune responses. However, their role in modulating tumor metastasis is still unclear. Here, we identify a conserved linear epitope-based peptide, Ma3P, located in the proteolytic region of major histocompatibility complex (MHC) class I-related chain A (MICA) α3 and further design mCM10-L, an mRNA vaccine that encodes the carrier protein CRM197 and 10 tandem repeats of Ma3P. We demonstrate that vaccination with mCM10-L induces the production of specific antibodies that block MICA/B α1/2 shedding, activate $CD8^+$ T cells and natural killer (NK) cells, and significantly inhibit $MICA/B^+$ tumor metastasis in mice. Furthermore, mCM10-L stimulation triggers the production of specific antibodies to promote MICA/B-mediated immune killing in an *in-vitro*-interacting human organoid model and humanized mice. Our results indicate the potential clinical application prospects of the mCM10-L vaccine.

INTRODUCTION

Tumor metastasis is the main cause of poor prognosis in patients with cancer. Immunotherapy has become the preferred strategy for preventing systemic metastasis, exerting effects mainly by enhancing immune surveillance to control and eliminate disseminated tumor cells.[1,2] Major histocompatibility complex (MHC) class I-related chain A/B (MICA/B) is one of the most important ligands of the activating receptor natural killer group 2 member D (NKG2D) on the surface of cytotoxic immune cells. As a stress-induced protein, MICA/B is highly expressed in a variety of solid tumors and hematological malignancies.[3–5] The extracellular region of MICA/B is composed of three domains, among which the α1/2 domain located at the distal membrane binds to NKG2D and provides a costimulatory signal to trigger T cell receptor-dependent cytotoxicity.[6] The α3 domain located in the proximal membrane contains multiple protease cleavage sites that are susceptible to hydrolysis; cleavage at these sites results in detachment of the α1/2 domain from the cell membrane and formation of an immunosuppressive soluble MICA/B (sMICA/B) protein, which downregulates NKG2D through competitive binding, blocking, and internalization and ultimately promotes tumor immune escape.[7–10] Unlike the highly polymorphic α1/2 domain, the α3 domain is relatively conserved. Antibodies targeting MICA/B α3 have been shown to inhibit MICA/B α1/2 shedding via steric hindrance.[11–13] Combined treatment with histone deacetylase inhibitors that increase MICA/B expression or anti-NKG2A antibodies that block natural killer (NK) cell inhibitory signals can further enhance the antitumor effect of anti-MICA/B α3 antibodies.[14,15] However, the process of tumor metastasis *in vivo* is insidious, and the occurrence of MICA/B α1/2 shedding is also difficult to capture. Anti-MICA/B α3 antibodies need to be used regularly, and drug resistance is common, making tumor immune escape difficult to combat.[16] Hence, tumor vaccines that can induce durable or even lifelong immune memory and initiate an active immune response in a timely manner to produce endogenous antibodies have considerable advantages in this regard, but no tumor vaccine targeting MICA/B has been approved for use.[17,18]

A recombinant protein consisting of MICA/B fused to lumazine synthase from *Brucella* spp. and a 24-polymer protein consisting

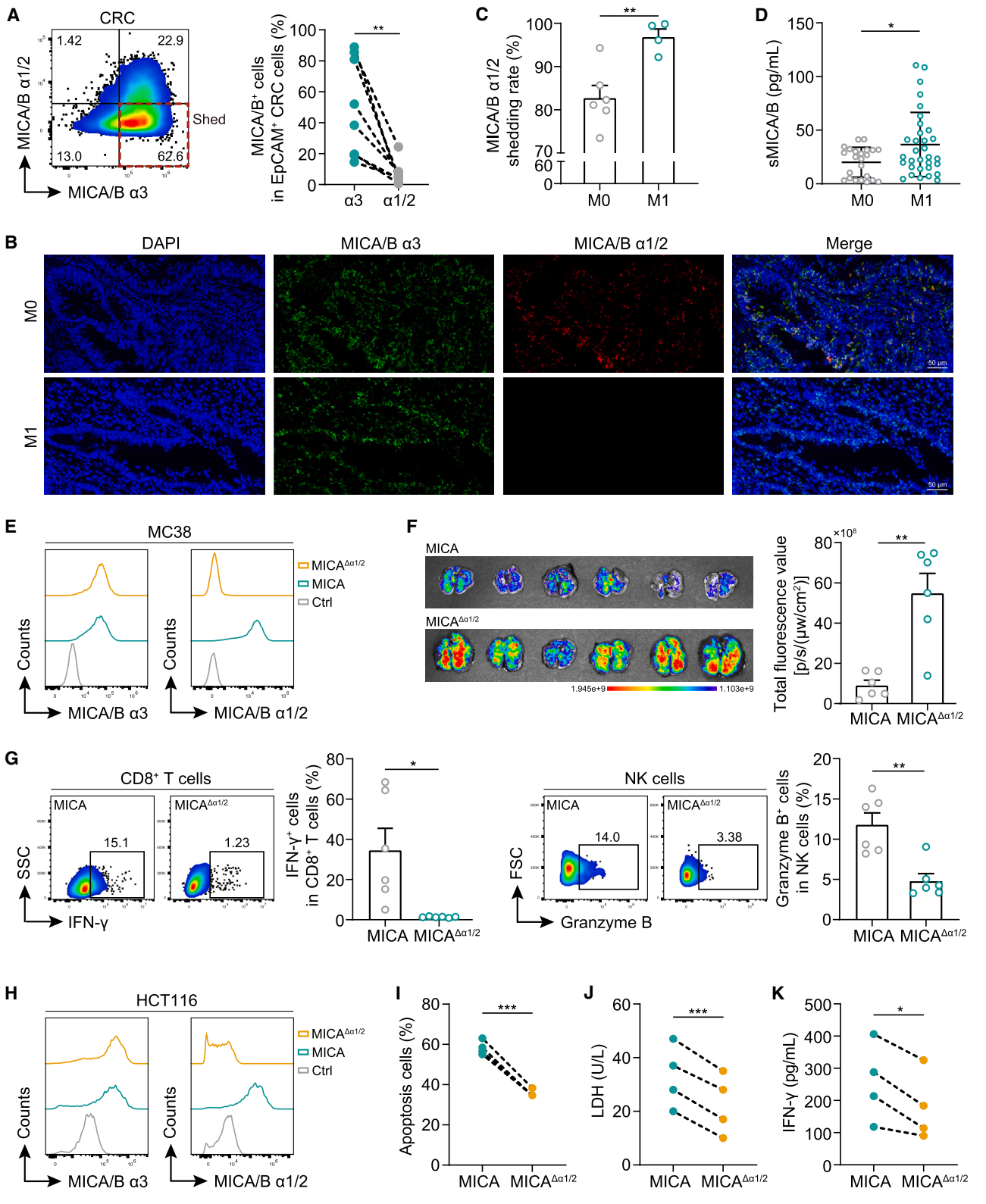

(legend on next page)

of the MICA/B α3 domain fused to the N terminus of ferritin from *Helicobacter pylori* have been reported to be used as antigens.[19,20] The corresponding vaccines have shown satisfactory results in animal models, but as a core component, macromolecular protein antigens may harbor undesirable or "useless" epitopes that can trigger unintentional and nonspecific immune responses and increase the potential risks of vaccine use.[21–23] Therefore, a precise coding sequence design based on combining the key epitopes of tumor antigens has the potential to improve the specificity of vaccines, thereby enhancing their antitumor effects and alleviating side effects.

mRNAs have recently attracted extensive attention as new therapeutic molecules that can transmit genetic information. Unlike DNA, mRNAs can be translated into almost all proteins or peptides without entering the nucleus, resulting in relatively high transfection efficiency and a low risk of accidental infection or opportunistic insertion mutations. Unlike conventional protein and peptide antigens, mRNAs can be translated sustainably without the need for large doses.[24–28] Since the remarkable success of such vaccines in combating the coronavirus disease 2019 pandemic, the development of mRNA-lipid nanoparticle (LNP) vaccines that target diverse tumors has become a popular direction in immunotherapy research. Thus, we aimed to develop an mRNA-LNP vaccine, mCM10-L, on the basis of a conserved B cell epitope-derived antigenic polypeptide located in the proteolytic region of MICA α3 and explore its inhibitory effect on tumor metastasis.

Our studies demonstrated that mCM10-L induced the production of specific antibodies that blocked the shedding of MICA/B α1/2, activated NK cells and $CD8^+$ T cells, and inhibited the metastasis of MICA/B^+ tumor cells. In addition, mCM10-L elicited the production of specific antibodies to promote MICA/B-mediated immune killing in a human immune organoid-tumor organoid-peripheral blood mononuclear cell (PBMC) interaction model *in vitro* and a hematopoietic stem cell (HSC)-humanized mouse model *in vivo*, highlighting the potential application prospects of this mRNA tumor vaccine.

RESULTS

MICA/B α1/2 shedding from tumor cell membranes promoted metastasis

Tumor cells secrete a variety of proteases to promote the hydrolysis of MICA/B on the cell membrane surface. To investigate the shedding of MICA/B α1/2 from tumor cells and its effect on metastasis, we first collected fresh tumor tissues from patients with colorectal cancer (CRC) and prepared single-cell suspensions by enzyme-free treatment (Figures S1A and S1B). Flow cytometry (FCM) revealed that the abundance of MICA/B α3 on the membrane of human CRC cells was significantly greater than that of MICA/B α1/2 (Figure 1A). Similar results were obtained in the subcutaneous tumor model using MICA/B^+ human primary CRC cells (Figure S1C).

Next, we evaluated the shedding of MICA/B α1/2 involved in tumor metastasis. Tumor tissues from patients with T3-stage CRC were collected, and immunofluorescence (IF) staining revealed that the shedding rate of MICA/B α1/2 on tumors in patients with distant metastasis (M1-stage) was significantly greater than that in patients without metastasis (M0-stage) (Figures 1B and 1C). Meanwhile, the serum concentration of sMICA/B in patients with T3-stage CRC yielded consistent results (Figure 1D). Then, we established enhanced green fluorescent protein (EGFP)$^+$ mouse colon adenocarcinoma MC38 cells expressing human full-length MICA or the MICA$^{\Delta\alpha1/2}$ mutant (Figure 1E). After the cells were administered separately to the mice via the tail vein, the lung metastases formed by tumor cells lacking MICA/B α1/2 expression were visibly larger (Figure 1F), and the killing activities of infiltrating $CD8^+$ T cells and NK cells were weakened (Figure 1G).

Finally, EGFP$^+$ human colon cancer HCT116 cells expressing human MICA or MICA$^{\Delta\alpha1/2}$ were constructed and cocultured with healthy human-derived PBMCs *in vitro* (Figure 1H). EGFP$^+$ tumor cell apoptosis and lactate dehydrogenase (LDH) and interferon-γ (IFN-γ) levels in the culture supernatants were evaluated, and the results revealed that the cytotoxic effect of PBMCs on MICA$^{\Delta\alpha1/2}$-expressing tumor cells was significantly weaker than that on MICA-expressing tumor cells (Figures 1I–1K).

Taken together, these data suggested that the α1/2 domain was shed from MICA/B^+ tumor cells and that this shedding attenuated immune attacks and promoted tumor metastasis.

Blocking the shedding of MICA/B α1/2 inhibited the metastasis of MICA/B^+ tumor cells

Proteolysis in the α3 domain initiates the shedding of MICA/B α1/2. Therefore, we prepared a murine monoclonal antibody targeting MICA/B α3 (termed MIA-2) via the traditional hybridoma method. MIA-2 effectively inhibited the shedding of MICA/B

Figure 1. MICA/B α1/2 shedding from tumor cell membranes promoted metastasis

(A) Representative (left) and quantification (right) of FCM for MICA/B α3 and α1/2 expression on the membrane of EpCAM$^+$ tumor cells in CRC tissues (n = 8).

(B and C) Representative (B) and quantification (C) of IF staining for MICA/B α3 (green) and α1/2 (red) in CRC tumors from T3M0-stage (n = 6) and T3M1-stage (n = 4) patients. Scale bar, 50 μm. MICA/B α1/2 shedding rate: $(1\text{-}Area\%_{\alpha1/2}/Area\%_{\alpha3}) \times 100\%$.

(D) The sMICA/B concentration in the serum of T3M0-stage (n = 23) and T3M1-stage (n = 32) patients with CRC was measured by ELISA.

(E–G) EGFP$^+$ MC38 cells stably expressing human full-length MICA or MICA$^{\Delta\alpha1/2}$ were validated by FCM (wild-type MC38 cells as negative controls) (E) and injected into C57BL/6 mice (n = 6 per group) via the tail vein. Lungs were collected 25 days post tumor inoculation, and the tumor burden, expressed as the total fluorescence value (Ex:480 nm/Em:520 nm), was assessed (F). Single-cell suspensions prepared from the lungs were stimulated with Cell Activation Cocktail (with BFA) for 6 h. The levels of IFN-γ secreted by $CD8^+$ T cells and granzyme B secreted by NK cells were determined by FCM (G).

(H–K) EGFP$^+$ HCT116 cells stably expressing human full-length MICA or MICA$^{\Delta\alpha1/2}$ were validated by FCM (wild-type HCT116 cells as negative controls) (H). These two types of cells were cocultured with PBMCs isolated from healthy individuals (n = 4) at a 1:10 ratio for 4 to 6 h. The apoptosis of EGFP$^+$ tumor cells was tested by FCM (I), the content of LDH released into the medium was measured via spectrophotometry (J), and the concentration of secreted IFN-γ in the medium was evaluated by FCM (K).

Data are presented as the mean ± SDs and were analyzed by paired Student's t test (A and I–K) or unpaired Student's t test (C, D, F, and G). $^*p < 0.05$, $^{**}p < 0.01$, and $^{***}p < 0.001$. See also Figure S1.

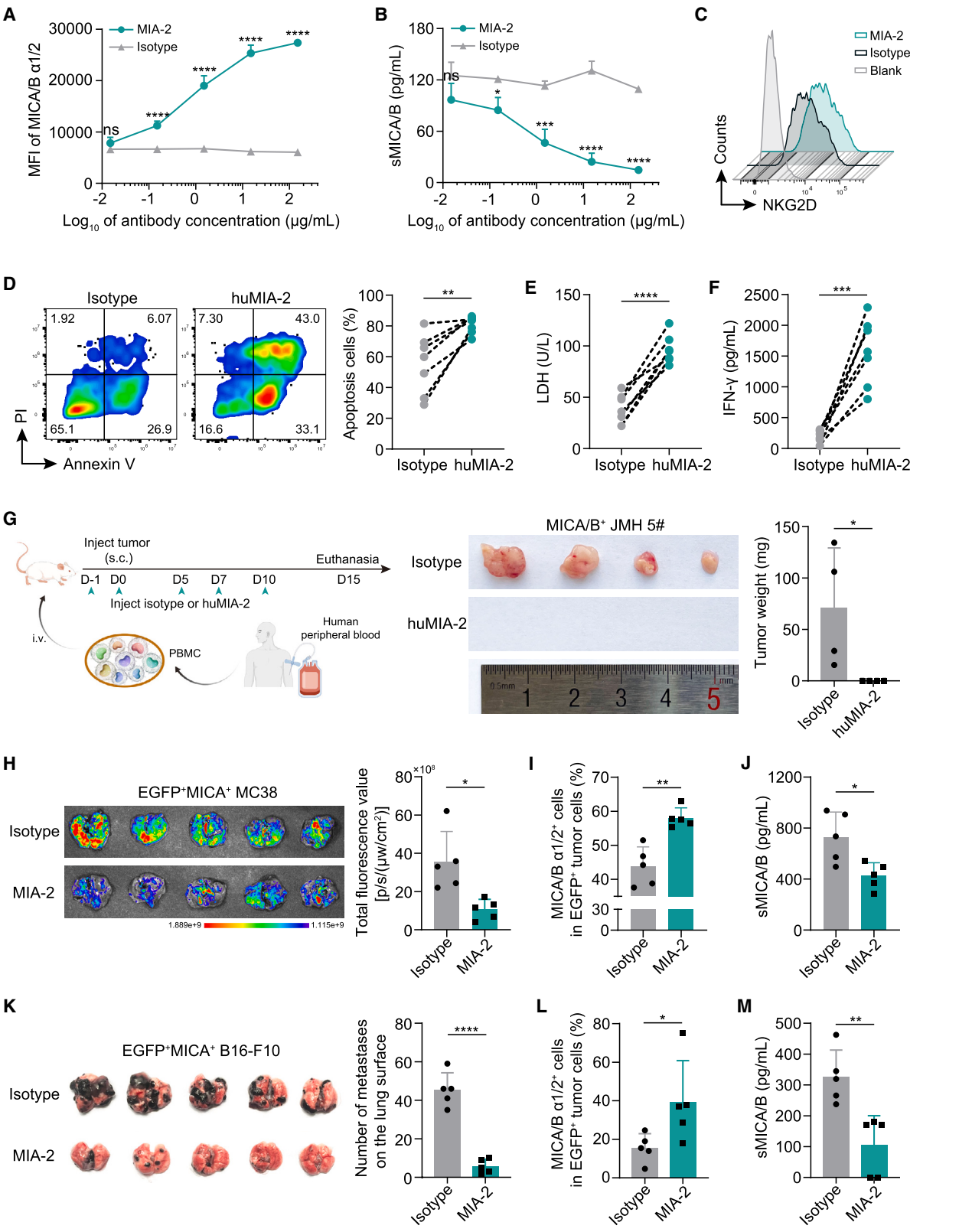

(legend on next page)

α1/2 from the cell membrane surface, and the binding of MIA-2 to MICA/B α3 did not affect the binding of MICA/B α1/2 to NKG2D (Figures 2A–2C). To characterize the immunological function of this antibody compatibly, we added humanized MIA-2 (huMIA-2) to an *in vitro* coculture system of EGFP$^+$ MICA$^+$ HCT116 cells with healthy human-derived PBMCs. HuMIA-2 dramatically promoted the apoptosis of EGFP$^+$ tumor cells and increased the levels of LDH and IFN-γ released into the supernatant (Figures 2D–2F). Furthermore, huMIA-2 markedly or even completely inhibited the growth of MICA/B$^+$ human primary CRC cells in PBMC-humanized C-NKG mice *in vivo* (Figures 2G and S2A–S2D). These results suggested that targeted blockade of MICA/B α1/2 shedding increased the cytotoxic effect of human-derived immune cells.

To investigate whether specific blockade of MICA/B α1/2 shedding via MIA-2 could inhibit tumor metastasis, we established a lung metastasis model in C57BL/6 mice using EGFP$^+$MICA$^+$ MC38 cells. Although the mouse genome does not contain *MICA/B*, human MICA/B α1/2 can typically activate mouse NKG2D.[11] Intraperitoneal injection of MIA-2 clearly relieved lung metastases in mice, increased the level of MICA/B α1/2 on metastatic EGFP$^+$ tumor cell membranes, and decreased the concentration of sMICA/B in the serum (Figures 2H–2J). Consistent results were replicated in a lung metastasis model using EGFP$^+$MICA$^+$ mouse melanoma B16-F10 cells (Figures 2K–2M). These data suggested that targeted blockade of MICA/B α1/2 shedding inhibited the metastasis of MICA/B$^+$ tumor cells.

Identification of a linear B cell epitope in the MICA α3 proteolytic region

The aforementioned findings indicated that the epitope specifically recognized by MIA-2 may be a dominant sequence for the development of tumor vaccines. To identify this epitope, we first designed four truncated MICA α3 mutants, T1–T4, with gradually shortened N termini, considering (1) the disulfide bond position (C23/C80), which may affect the spatial conformation of the protein, and (2) the three potential regions (S12-G17, V42-G60, or S85-H109) indicated by the linear B cell epitope prediction from the Immune Epitope Database (prediction score >0.5) (Figures 3A, S3A, and S3B). ELISA revealed that the binding of MIA-2 to T1 was decreased compared with that to MICA α3 but was similar to that to T2 and that the binding of MIA-2 to T3 was decreased compared with that to T2 but was similar to that to T4 (Figure 3B). These results suggested that the epitope recognized by MIA-2 might be located in the R01-V21 or V42-G58 region of MICA α3. We further constructed a spliced MICA α3 mutant, D1, with deletion of T22-C80 and a spliced MICA α3 mutant, D2, with deletion of V42-G58 (Figures 3A and S3C). ELISA revealed that neither of these mutants could bind to MIA-2, demonstrating that the epitope of MIA-2 was located at V42-G58 and that the decrease in its T1 binding capacity might be related to a decrease in affinity induced by the conformational change (Figure 3C). We then constructed six spliced MICA α3 mutants, D3–D8, with the length of the deletion gradually decreased at the N- or C terminus (Figures 3A and S3C). ELISA revealed three main findings: (1) the binding of MIA-2 to D4 was similar to that to D3, indicating that the epitope did not contain G52-L55; (2) the binding of MIA-2 to D5 was greater than that to D4 but similar to that to D6, indicating that the epitope was located at the C terminus of the deleted region of D4; and (3) the binding of MIA-2 to D6, D7, and D8 gradually increased, with its binding to D8 equivalent to its binding to MICA α3, suggesting that the epitope was located at S45-W51 of MICA α3 (Figure 3D).

Next, to further pinpoint the epitope recognized by MIA-2, we conjugated the macromolecular carrier protein bovine serum albumin (BSA) to the C or N terminus of this chemically synthesized peptide—SHDTQQW (termed PEP). ELISA revealed that the C-terminal-conjugated peptide but not the N-terminal-conjugated peptide could bind to MIA-2, implying that exposure of S45 located at the N terminus was key to MIA-2 recognition

Figure 2. Blocking the shedding of MICA/B α1/2 inhibited the metastasis of MICA/B$^+$ tumor cells

(A and B) MIA-2 or the isotype control (150, 15, 1.5, 0.15, and 0.015 μg/mL) was added to the culture medium of A375 cells and incubated overnight. The expression of MICA/B α1/2 on the cell membrane was evaluated by FCM (A), and the concentration of sMICA/B shed into the medium was measured by ELISA (B). $n = 3$ independent experiments.

(C) A375 cells were treated with 10 μg/mL MIA-2 or the isotype control and then incubated with 10 μg/mL recombinant NKG2D protein. The level of NKG2D bound to the cell membrane surface was evaluated by FCM. $n = 3$ independent experiments.

(D–F) HuMIA-2 or the isotype control (10 μg/mL) was added to the culture medium of EGFP$^+$MICA$^+$ HCT116 cells and incubated overnight. The cells were then cocultured with PBMCs isolated from healthy individuals ($n = 7$) at a 1:10 ratio for 4 to 6 h. The apoptosis of EGFP$^+$ tumor cells was evaluated by FCM (D), the content of LDH released into the medium was determined via spectrophotometry (E), and the concentration of secreted IFN-γ in the medium was evaluated by FCM (F).

(G) MICA/B$^+$ JMH 5# cells were subcutaneously inoculated into PBMC-humanized C-NKG mice ($n = 4$ per group) to establish a subcutaneous tumor model. HuMIA-2 or the isotype control was intraperitoneally injected (200 μg per mouse) on days −1, 0, 5, 7, and 10, as described. Following experimental termination, the subcutaneous tumors were harvested, photographed, and weighed.

(H–J) EGFP$^+$MICA$^+$ MC38 cells were injected into C57BL/6 mice ($n = 5$ per group) via the tail vein to establish a lung metastasis model, and MIA-2 or the isotype control was intraperitoneally injected (200 μg per mouse) on days −1, 0, 5, 7, and 10. Lungs were collected 25 days post tumor inoculation, and the tumor burden, expressed as the total fluorescence value (Ex:480 nm/Em:520 nm), was assessed (H). The level of MICA/B α1/2 on the membrane of EGFP$^+$ tumor cells in the lungs was evaluated by FCM (I), and the concentration of sMICA/B in the serum was measured by ELISA (J).

(K–M) EGFP$^+$MICA$^+$ B16-F10 cells were injected into C57BL/6 mice ($n = 5$ per group) via the tail vein to establish a lung metastasis model, and MIA-2 or the isotype control was intraperitoneally injected (200 μg per mouse) on days −1, 0, 5, 7, and 10. Lungs were collected 25 days post tumor inoculation, and the number of metastatic lesions on the surface was recorded (K). The level of MICA/B α1/2 on the membrane of EGFP$^+$ tumor cells in the lungs was evaluated by FCM (L), and the concentration of sMICA/B in the serum was measured by ELISA (M).

Data are presented as the mean ± SDs and were analyzed by two-way ANOVA (A and B), paired Student's *t* test (D–F), or unpaired Student's t test (G–M). ns: no significant difference, $^*p < 0.05$, $^{**}p < 0.01$, $^{***}p < 0.001$, and $^{****}p < 0.0001$. See also Figure S2.

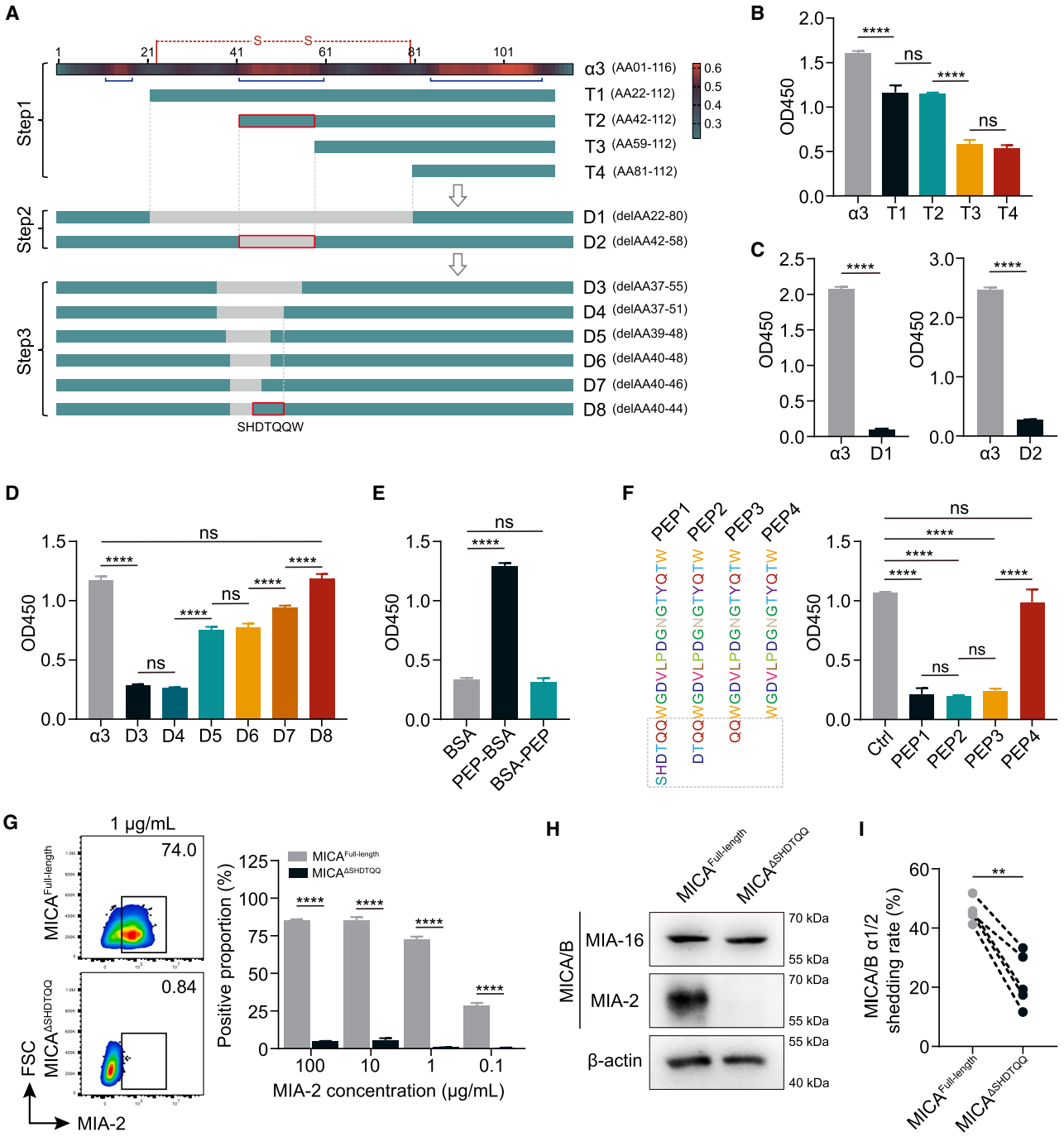

Figure 3. Identification of a linear B cell epitope in the MICA α3 proteolytic region

(A) Workflow for preliminary epitope identification and schema for T1–T4 and D1–D8 mutants. MICA α3 is represented via a heatmap based on the prediction score of amino acids by the IEDB (http://www.iedb.org), with blue underlines indicating potential linear B cell epitopes. Deleted regions are marked in gray, and identified peptides are marked in red boxes.

(B–D) The binding levels of MIA-2 to MICA α3, T1–T4 (B), D1-D2 (C), and D3–D8 (D) were determined by ELISA. *n* = 3 independent experiments.

(E) BSA was conjugated to the C terminus (PEP-BSA) and N terminus (BSA-PEP) of SHDTQQW. The binding levels of MIA-2 to BSA, PEP-BSA, and BSA-PEP were determined by ELISA. *n* = 3 independent experiments.

(F) Amino acid sequence of PEP1–PEP4 (left). After prereacting MIA-2 with PEP1–PEP4 at 37°C for 1 h, the binding levels of MIA-2 to MICA α3 were determined by ELISA, with an equal volume of PBS as a positive control. *n* = 3 independent experiments.

(G) *MICA*$^{Full\text{-}length}$ or *MICA*$^{\Delta SHDTQQ}$ expression plasmids were transfected into HEK293T cells. Representative (left) and quantification (right) of FCM for MIA-2 (100, 10, 1, and 0.1 μg/mL) binding to the membranes of MICA$^{Full\text{-}length}$-expressing and MICA$^{\Delta SHDTQQ}$-expressing cells. *n* = 3 independent experiments.

(legend continued on next page)

(Figure 3E). Moreover, we synthesized four peptides, PEP1–PEP4, with gradual deletion of the SHDTQQ sequence (Figure 3F, left). After coincubation of each peptide separately with MIA-2, ELISA revealed that PEP1–PEP3 but not PEP4 blocked the binding of MIA-2 to MICA α3, confirming that S45-Q50 are the key amino acids recognized by MIA-2 (Figure 3F, right).

Finally, the expression plasmid for the SHDTQQ-deleted MICA mutant (*MICA*$^{\Delta SHDTQQ}$) was constructed and transiently transfected into HEK293T cells, and the *MICA*$^{Full\text{-}length}$ plasmid with equivalent transfection efficiency was used as a positive control (Figure S3D). FCM and western blot analysis revealed that MIA-2 clearly bound to MICA$^{Full\text{-}length}$ but not to MICA$^{\Delta SHDTQQ}$ (Figures 3G, 3H, and S3E). Additionally, when both types of HEK293T cells were incubated with 100% fresh human serum containing proteases, FCM revealed a lower shedding rate of MICA α1/2 in MICA$^{\Delta SHDTQQ}$-expressing cells compared to MICA$^{Full\text{-}length}$-expressing cells (Figure 3I). These results proved that SHDTQQ was a linear B cell epitope located in the proteolytic region of MICA α3.

The antigenic peptide designed on the basis of the aforementioned epitope activated CD8$^+$ T cell-mediated antitumor immunity by inducing the production of specific antibodies

On the basis of the B cell epitope identified earlier, we lengthened the sequence at both ends to protect its structural features, in which we avoided possible glycosylation sites and added potential human CD4$^+$ T cell epitopes and CD8$^+$ T cell epitopes inferred by computer-aided simulation (Figures S4A and S4B). A 22-amino acid antigenic peptide (SWRQDGVSLSHDTQQWG DVLPD) was then designed and named the MICA α3 peptide (termed Ma3P) (Figure 4A). Analysis via the Immuno-Polymorphism Database-international ImMunoGeneTics project (IPD-IMGT)/human leukocyte antigen (HLA) database revealed that the Ma3P sequence was relatively conserved in prevalent MICA alleles (Figure S4C). Then, we isolated PBMCs from a healthy donor with HLA-A*24:03(+)/A*33(−) and HLA-DRB1*08(−)/DRB1*12(−) alleles and stimulated them with Ma3P. FCM revealed an increase in IFN-γ level produced by CD8$^+$ T cells but not CD4$^+$ T cells, suggesting the accuracy of human T cell epitope prediction in Ma3P (Figure S4D).

First, to verify the immunogenicity of Ma3P, we mixed Ma3P with Quil A (termed Ma3P-Q), a commonly used veterinary adjuvant that is beneficial for increasing antibody titers, and immunized C57BL/6 mice with this mixture via subcutaneous injection (Figure 4B). Five days after the second immunization, the presence of specific anti-MICA IgG and IgM antibodies was detected in the serum of Ma3P-Q-immunized mice (Figure 4C), and the expression of MICA/B α1/2 on the membrane of human tumor cells was increased by incubation with this serum *ex vivo* (Figure 4D). We also collected mice splenocytes. FCM revealed an increase in IFN-γ secretion by CD4$^+$ T cells and CD8$^+$ T cells after Ma3P-Q immunization, but IFN-γ secretion did not further increase after *ex vivo* stimulation with Ma3P (Figure S4E). Moreover, the clearance of CD4$^+$ T cells during immunization had no effect on the amount of Ma3P-induced specific anti-MICA antibodies (Figure 4E). These findings suggested that Ma3P was able to induce the production of specific antibodies that block MICA/B α1/2 shedding through its B cell epitope but was unable to activate specific cellular immunity due to the absence of CD4$^+$ T cell epitopes or CD8$^+$ T cell epitopes in C57BL/6 mice.

Next, to evaluate the effect of Ma3P vaccination on MICA/B$^+$ tumor cell metastasis, we established a lung metastasis model in C57BL/6 mice via tail vein injection of EGFP$^+$MICA$^+$ MC38 cells after secondary immunization with Ma3P-Q and found that the Ma3P-Q group had fewer metastases and more infiltrating CD8$^+$ T cells and NK cells in the lungs than did the control group. However, this change was abrogated after B cells were pre-eliminated *in vivo* with an anti-B220 antibody, which prevented the production of anti-MICA antibodies (Figures 4F, 4G, and S4F). These results suggested that Ma3P vaccination inhibited tumor metastasis by triggering B cell immunity. Then, we utilized the same lung metastasis model but administered an anti-CD8a antibody or anti-NK1.1 antibody after secondary immunization and before tumorigenesis. The antitumor effect of Ma3P vanished after depletion of CD8$^+$ T cells but still occurred after depletion of NK cells (Figure 4H), indicating that CD8$^+$ T cells were the key effector cells in Ma3P vaccination and that the underlying mechanism was presumably that Ma3P can activate the MICA-NKG2D costimulatory signal of CD8$^+$ T cells by inducing the production of specific antibodies.

Finally, to test the antimetastatic effect of Ma3P vaccination on other tumor types, we constructed a lung metastasis model using EGFP$^+$MICA$^+$ B16-F10 cells in C57BL/6 mice. Compared with the control group, the Ma3P-Q group presented a decrease in the number of lung metastases (Figure 4I), an increase in the expression of MICA/B α1/2 on the surface of EGFP$^+$ tumor cells (Figure 4J), a decrease in the serum concentration of sMICA/B (Figure 4K), and a considerable increase in the cytotoxic activity of CD8$^+$ T cells in peripheral blood (Figure 4L). These results demonstrated that Ma3P vaccination effectively suppressed the metastasis of MICA/B$^+$ tumor cells.

The mRNA-LNP vaccine encoding Ma3P triggered specific antimetastatic immune activity in mice

To optimize the antigen format and delivery method, we developed an mRNA-LNP vaccine expressing the nontoxic cross-reactive molecule diphtheria toxin 197 (CRM197) and 10 tandem repeats of Ma3P, named mRNA-CRM197-Ma3P *10-LNP (mCM10-L) (Figure 5A). The same form of mRNA-LNP encoding a single Ma3P (termed mM1-L) was used as a control. mCM10-L induced the production of specific anti-MICA antibodies after

(H) Western blot for MIA-2 binding to MICA$^{Full\text{-}length}$ and MICA$^{\Delta SHDTQQ}$ proteins, with an anti-MICA/B α1/2 antibody (clone: MIA-16) as a positive control. $n = 3$ independent experiments.

(I) MICA$^{Full\text{-}length}$-expressing and MICA$^{\Delta SHDTQQ}$-expressing HEK293T cells were incubated with 100% fresh human serum containing proteases ($n = 5$ donors) at 37°C for 30 min. The expression of MICA/B α1/2 on the cell membrane was detected by FCM. MICA/B α1/2 shedding rate: $(1\text{-}MFI_{treated}/MFI_{untreated}) \times 100\%$. Data are presented as the mean ± SDs and were analyzed by one-way ANOVA (B and D–F), unpaired Student's t test (C), two-way ANOVA (G), or paired Student's t test (I). ns: no significant difference, $^{**}p < 0.01$ and $^{****}p < 0.0001$. See also Figure S3.

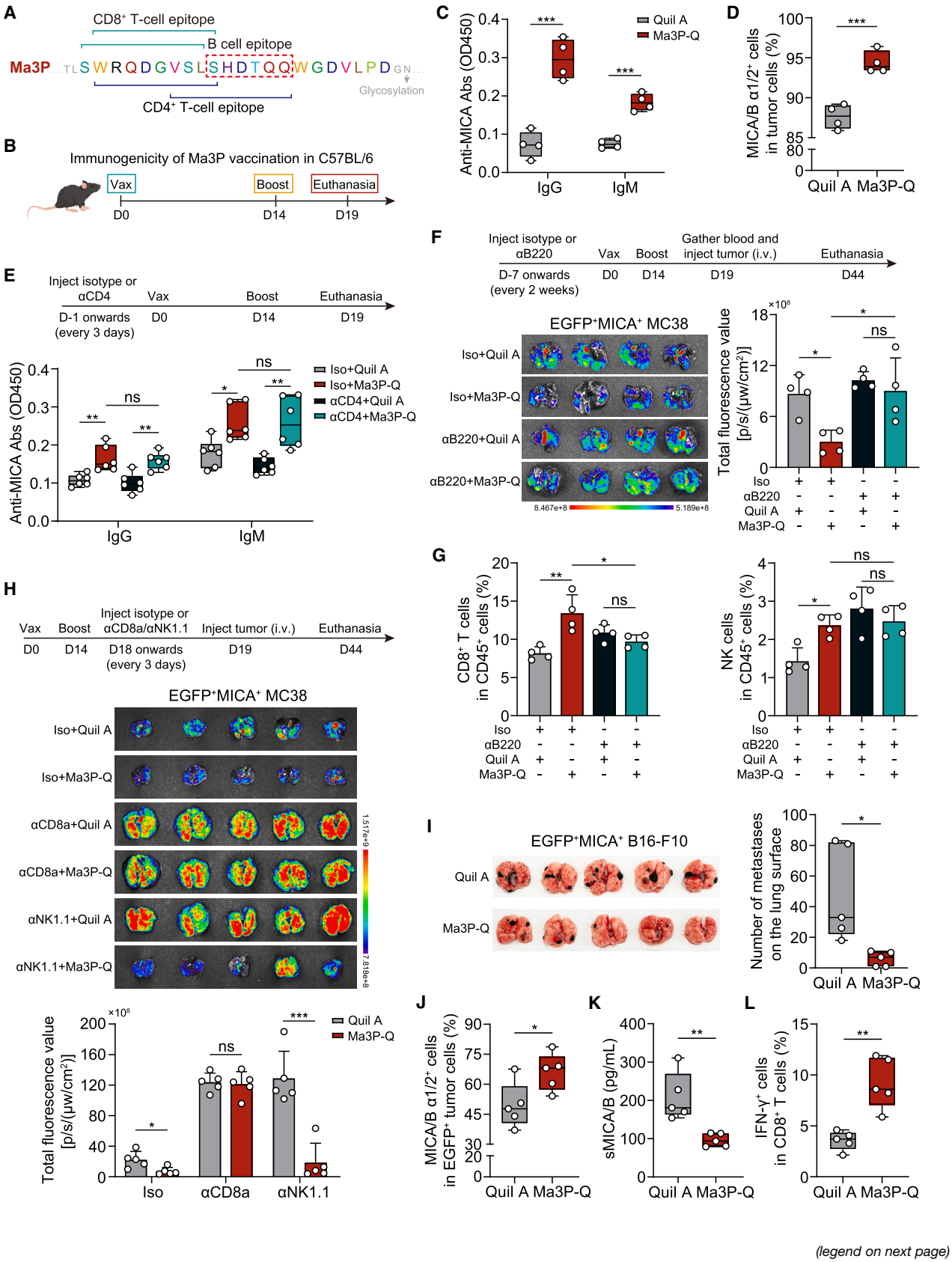

(legend on next page)

two immunizations via intramuscular injection in C57BL/6 mice, whereas mM1-L did not (Figure 5B). Furthermore, the level of MICA/B α1/2 on the membranes of human tumor cells increased after the *ex vivo* addition of serum from mCM10-L group mice into the medium (Figure 5C).

Next, to test whether mCM10-L exerts an antimetastatic effect *in vivo* and benchmark it against vaccines that were developed based on the validated MICA α3 antigen, we designed an mRNA-LNP expressing CRM197 fused with MICA α3 (termed mCa3-L) and an mRNA-LNP expressing MICA α3 alone (termed ma3-L) as controls, and all three were found to produce comparable levels of specific anti-MICA IgG antibody after immunization (Figure 5D). Then, we established a lung metastasis model using EGFP$^+$MICA$^+$ MC38 cells in vaccinated mice and found that mCM10-L, like mCa3-L and ma3-L, strongly suppressed tumor metastasis, suggesting that mCM10-L, which expressed only B cell epitopes of MICA α3, had a non-inferior antimetastatic effect compared with those of similar vaccines expressing intact MICA α3 (Figures 5E and S5A).

Third, to evaluate the change of immune microenvironment during the colonization of metastatic tumors after vaccination with mCM10-L, we harvested the lung tissues from the aforementioned tumor-bearing mice in the mCM10-L group and control group and prepared single-cell suspensions. Eight samples were examined via cytometry by time of flight (CyTOF), and 27 cell clusters were identified using 42 immunophenotypes (Figure S5B). Within the clusters, we defined several known cell types. Overall, mCM10-L significantly increased the proportion of CD4$^+$ T cells, $\gamma\delta$T cells, NK cells, and monocytes and decreased the proportion of macrophages, while a slight increase in myeloid-derived suppressor cells (MDSCs) was accompanied (Figure 5F). Although there was no evident change in the proportion of infiltrating CD8$^+$ T cells, further analysis of this subset revealed that the expression of immune checkpoints programmed cell death protein-1 (PD-1; CD279), lymphocyte activation gene-3 (LAG-3; CD223), and T cell immunoglobulin and mucin domain-containing protein 3 (TIM-3; CD366) was downregulated in the mCM10-L group (Figure 5G). In addition, we isolated CD8$^+$ T cells and NK cells from the peripheral blood of tumor-bearing mice via magnetic beads and cocultured them with MC38 cells *ex vivo*. CD8$^+$ T cells and NK cells from the mCM10-L group both killed more tumor cells than those from the control group did (Figure S5C). Taken together, these data demonstrated that mCM10-L obviously reshaped the immune microenvironment during the antitumor process, including the mobilization of both NK cells and CD8$^+$ T cells.

Finally, we evaluated the efficacy of mCM10-L against other types of tumor metastasis. When we injected EGFP$^+$MICA$^+$ MC38 cells into mice through the tail vein and then inoculated them with mCM10-L twice after tumorigenesis for 5 days, the formation of lung metastases was still reduced (Figure 5H). This phenomenon was replicated in a lung metastasis model using EGFP$^+$MICA$^+$ B16-F10 cells (Figure S5D). Moreover, in the model of vaccination after the surgical removal of primary tumors established using luciferase$^+$MICA$^+$ mouse breast cancer 4T1 cells, mCM10-L also significantly slowed recurrence *in situ* and distant metastases (Figure 5I). Memory B cells (mainly IgM$^-$) increased after rechallenge with luciferase$^+$MICA$^+$ 4T1 cells in mCM10-L-vaccinated mice that remained tumor free (Figure S5E). These data indicated that mCM10-L had an impressive inhibitory effect on various types of MICA/B$^+$ tumor metastasis.

mCM10-L elicited a specific B cell antitumor response in human immune cell-based models

To evaluate the immunogenicity of mCM10-L in humans, fresh human tonsil samples were used to generate immune organoids *in vitro*, in which mRNA antigens were absorbed and expressed primarily in B cells, CD4$^+$ T cells, CD8$^+$ T cells, and plasma cells (Figures 6A and S6A). After stimulation with mCM10-L, B cell differentiation was increased, and anti-MICA huIgG antibody was

Figure 4. The antigenic peptide designed on the basis of the aforementioned epitope activated CD8$^+$ T cell-mediated antitumor immunity by inducing the production of specific antibodies

(A) Ma3P sequence. Potential human CD4$^+$ T cell epitopes and CD8$^+$ T cell epitopes are marked with square brackets.

(B) Ma3P-Q vaccination flow chart.

(C and D) Ma3P (20 μg/100 μL) was mixed with Quil A (7.5 μg/100 μL) and then injected subcutaneously into C57BL/6 mice (n = 4 per group) on days 0 and 14, with an equal volume of PBS mixed with Quil A as a control. Serum was collected 5 days post second immunization, and the levels of specific anti-MICA IgG and IgM antibodies in the serum (diluted 1:20) were measured by ELISA (C). Serum was then added at a 1:8 ratio to the medium of A375 cells and incubated overnight. The level of MICA/B α1/2 on the cell membrane was evaluated by FCM (D).

(E) Anti-CD4 antibody (αCD4) was injected intraperitoneally (200 μg per mouse) every 3 days starting 1 day before Ma3P-Q vaccination to eliminate CD4$^+$ T cells in C57BL/6 mice (n = 6 per group). Serum was collected 5 days post second immunization, and the levels of specific anti-MICA IgG and IgM antibodies in the serum (diluted 1:20) were measured by ELISA.

(F and G) Anti-B220 antibody (αB220) was injected intraperitoneally (200 μg per mouse) every 2 weeks starting 7 days before Ma3P-Q vaccination to pre-eliminate B cells in C57BL/6 mice (n = 4 per group). Five days post second immunization, EGFP$^+$MICA$^+$ MC38 cells were then injected into C57BL/6 mice via the tail vein to establish a lung metastasis model. Following experimental termination, the lungs were collected, and the tumor burden, expressed as the total fluorescence value (Ex:480 nm/Em:520 nm), was assessed (F). The percentages of CD8$^+$ T cells and NK cells infiltrated in lungs were determined by FCM (G).

(H) Anti-CD8 antibody (αCD8) or anti-NK1.1 antibody (αNK1.1) was injected intraperitoneally (200 μg per mouse) every 3 days to eliminate CD8$^+$ T cells or NK cells starting 1 day before EGFP$^+$MICA$^+$ MC38 cells were injected into Ma3P-Q-vaccinated C57BL/6 mice (n = 5 per group) via the tail vein. Following experimental termination, the lungs were collected, and the tumor burden, expressed as the total fluorescence value (Ex:480 nm/Em:520 nm), was assessed.

(I–L) EGFP$^+$MICA$^+$ B16-F10 cells were injected into Ma3P-Q-vaccinated C57BL/6 mice (n = 5 per group) via the tail vein. Lungs were collected 25 days post tumor inoculation, and the number of metastatic lesions on the surface was recorded (I). The level of MICA/B α1/2 on the membrane of EGFP$^+$ tumor cells in the lungs was evaluated by FCM (J), and the concentration of sMICA/B in the serum was measured by ELISA (K). Single-cell suspensions prepared from peripheral blood were stimulated with Cell Activation Cocktail (with BFA) for 6 h. The level of IFN-γ secreted by CD8$^+$ T cells was determined by FCM (L).

Data are presented as the mean ± SDs and were analyzed by unpaired Student's t test (C, D, and H–L) or one-way ANOVA (E–G). ns: no significant difference, $^*p < 0.05$, $^{**}p < 0.01$, and $^{***}p < 0.001$. See also Figure S4.

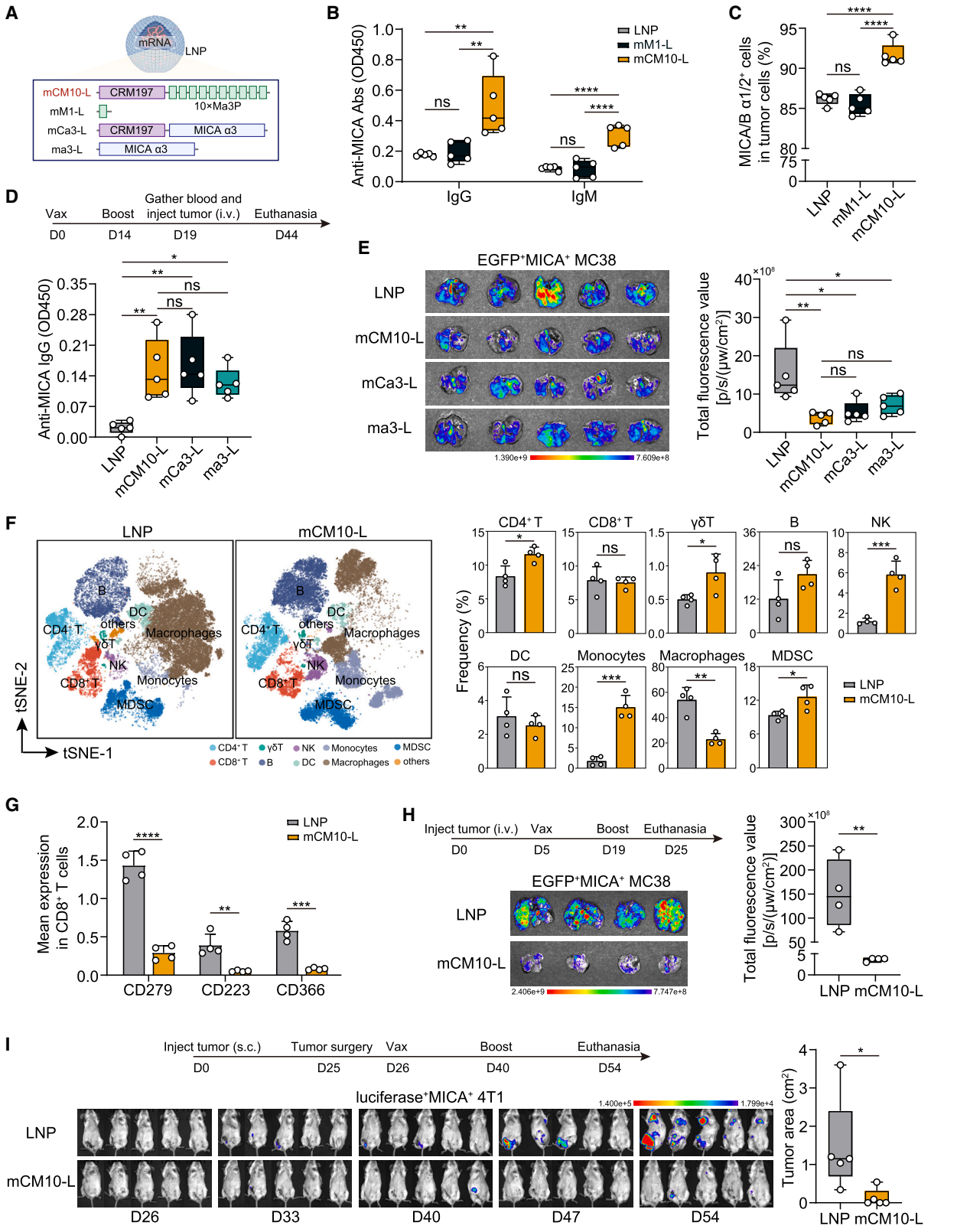

(legend on next page)

continuously secreted (Figures 6B and 6C). In a contactless coculture system of immune organoids with MICA/B$^+$ tumor cells, the levels of MICA/B α1/2 on tumor cell membranes increased after the addition of mCM10-L to the chamber (Figure 6D), indicating that mCM10-L could activate human-derived B cells to produce specific antibodies that block the shedding of MICA/B α1/2.

Furthermore, to investigate whether the antibodies induced by mCM10-L increase the tumoricidal activity of human immune cells, an innovative *in vitro* human immune organoid-CRC organoid-PBMC interaction model was constructed (Figures 6A and S6B). The anti-MICA antibodies secreted by mCM10-L-treated immune organoids also increased the levels of MICA/B α1/2 on the surface of tumor organoids (Figure S6C), and these tumor organoids were more susceptible to immune killing when cocultured with PBMCs isolated from patients with matched CRC (Figure 6E), suggesting that mCM10-L could enhance MICA/B-mediated antitumor effects by triggering a specific B cell immune response.

Lastly, HSC-humanized C-NKG mice were used to mimic the human immune response to mCM10-L inoculation *in vivo*, and specific anti-MICA huIgG antibody was present in the serum after two immunizations (Figures 6F and S6D). Compared with that in the control group, the formation of lung metastases was reduced in the mCM10-L group after the tail vein injection of EGFP$^+$MICA/B$^+$ human primary CRC cells into these mice (Figures 6G and S6E). Taken together, these data suggested that mCM10-L likely exhibited decent immunoreactivity in humans.

DISCUSSION

Humanized antibodies have become the primary and preferred strategy for cancer therapy, but they still have drawbacks, such as a short half-life and autoimmunogenicity. Compared with full-length protein vaccines, B cell epitope vaccines aim to continuously induce the production of protective endogenous antibodies and elicit more effective and safer immune responses against targeted antigenic regions, thus becoming a promising and cost-effective means to prevent cancer in humans.[29,30] However, only a few B cell epitope vaccines have been successfully developed and implemented.[31,32]

Here, we report an mRNA vaccine with the ability to trigger specific B cell-mediated antimetastatic activity. Specifically, we identified a linear B cell epitope located in the proteolytic region of MICA α3. On the basis of this epitope, we designed a conserved antigenic peptide, Ma3P, and demonstrated that Ma3P activated the CD8$^+$ T cell-mediated antitumor response *in vivo* by inducing the production of specific antibodies that block MICA/B α1/2 shedding, resulting in a robust capacity to inhibit the metastasis of MICA/B$^+$ tumor cells. Furthermore, we developed mCM10-L, an mRNA-LNP vaccine encoding CRM197 with 10 Ma3P repeats, which potently evoked specific antibodies to promote MICA/B-mediated immune killing in an *in-vitro*-interacting human organoid model and humanized mice. This study provides an ideal strategy for developing B cell epitope tumor vaccines.

Impairment of the MICA/B-NKG2D pathway is an important molecular mechanism employed by tumor cells to escape recognition and killing by immune cells and spread throughout the body.[33,34] MICA/B α3-targeted antibodies are currently recognized as a therapeutic approach. Consistent with previous studies, our MIA-2 antibody blocked the shedding of MICA/B α1/2 and significantly inhibited the metastasis of MICA/B$^+$ tumor cells in mice. However, tumor metastasis is insidious, with most patients with cancer developing metastatic lesions within months to years after resection of primary tumors, during which time the tumor cells remain largely dormant. Regulators in the premetastatic niche support the survival of potentially metastatic cells.[35] For example, latency competent cancer (LCC) cells that exhibit suspended animation can be isolated from human lung and breast cancer cell lines. Extensive downregulation of UL16-binding proteins (ULBP) ligands allows LCC cells to evade NK cell-mediated killing, thereby facilitating their survival in host organs under immune surveillance and providing opportunities for metastatic growth under appropriate conditions.[36] In line

Figure 5. The mRNA-LNP vaccine encoding Ma3P triggered specific antimetastatic immune activity in mice

(A) Architecture schema of mCM10-L, mM1-L, mCa3-L, and ma3-L.

(B and C) mM1-L or mCM10-L (3 μg/100 μL) was injected intramuscularly into C57BL/6 mice (n = 5 per group) on days 0 and 14, with an equal dose of LNPs as a control. Serum was collected 5 days post second immunization, and the levels of specific anti-MICA IgG and IgM antibodies in the serum (diluted 1:20) were measured by ELISA (B). Serum was then added at a 1:8 ratio to the medium of A375 cells and incubated overnight. The level of MICA/B α1/2 on the cell membrane was evaluated by FCM (C).

(D and E) mCM10-L, mCa3-L, or ma3-L (3 μg/100 μL) was injected intramuscularly into C57BL/6 mice (n = 5 per group) on days 0 and 14, with an equal dose of LNPs as a control. Serum was collected 5 days post second immunization, and the level of specific anti-MICA IgG antibody in the serum (diluted 1:20) was measured by ELISA (D). EGFP$^+$MICA$^+$ MC38 cells were then injected into vaccinated mice via the tail vein. Following experimental termination, the lungs were collected, and the tumor burden, expressed as the total fluorescence value (Ex:480 nm/Em:520 nm), was assessed (E).

(F and G) Single-cell suspensions of lungs from mCM10-L-vaccinated tumor-bearing mice and control mice (n = 4 per group) were analyzed via CyTOF. T-distributed stochastic neighbor embedding (t-SNE) plots (left) and statistical graphs (right) of the main subpopulation clusters (F). Statistical graphs of the mean expression level of CD279, CD223, and CD366 in the CD8$^+$ T cell subset (G).

(H) EGFP$^+$MICA$^+$ MC38 cells were first injected into C57BL/6 mice (n = 4 per group) via the tail vein. mCM10-L (3 μg/100 μL) was injected intramuscularly into tumor-bearing mice 5 days post tumor inoculation, with an equal dose of LNPs as a control. Following experimental termination, the lungs were collected, and the tumor burden, expressed as the total fluorescence value (Ex:480 nm/Em:520 nm), was assessed.

(I) BALB/c mice (n = 5 per group) were immunized with mCM10-L (3 μg/100 μL) following surgical removal of primary tumors constructed using luciferase$^+$MICA$^+$ 4T1 cells, with an equal dose of LNPs as a control. *In vivo* bioluminescence imaging was performed every 7 days after surgery, and the tumor burden, expressed as the total luminous area, was recorded.

Data are presented as the mean ± SDs and were analyzed by one-way ANOVA (B–E) or unpaired Student's t test (F–I). ns: no significant difference, $^*p < 0.05$, $^{**}p < 0.01$, $^{***}p < 0.001$, and $^{****}p < 0.0001$. See also Figure S5.

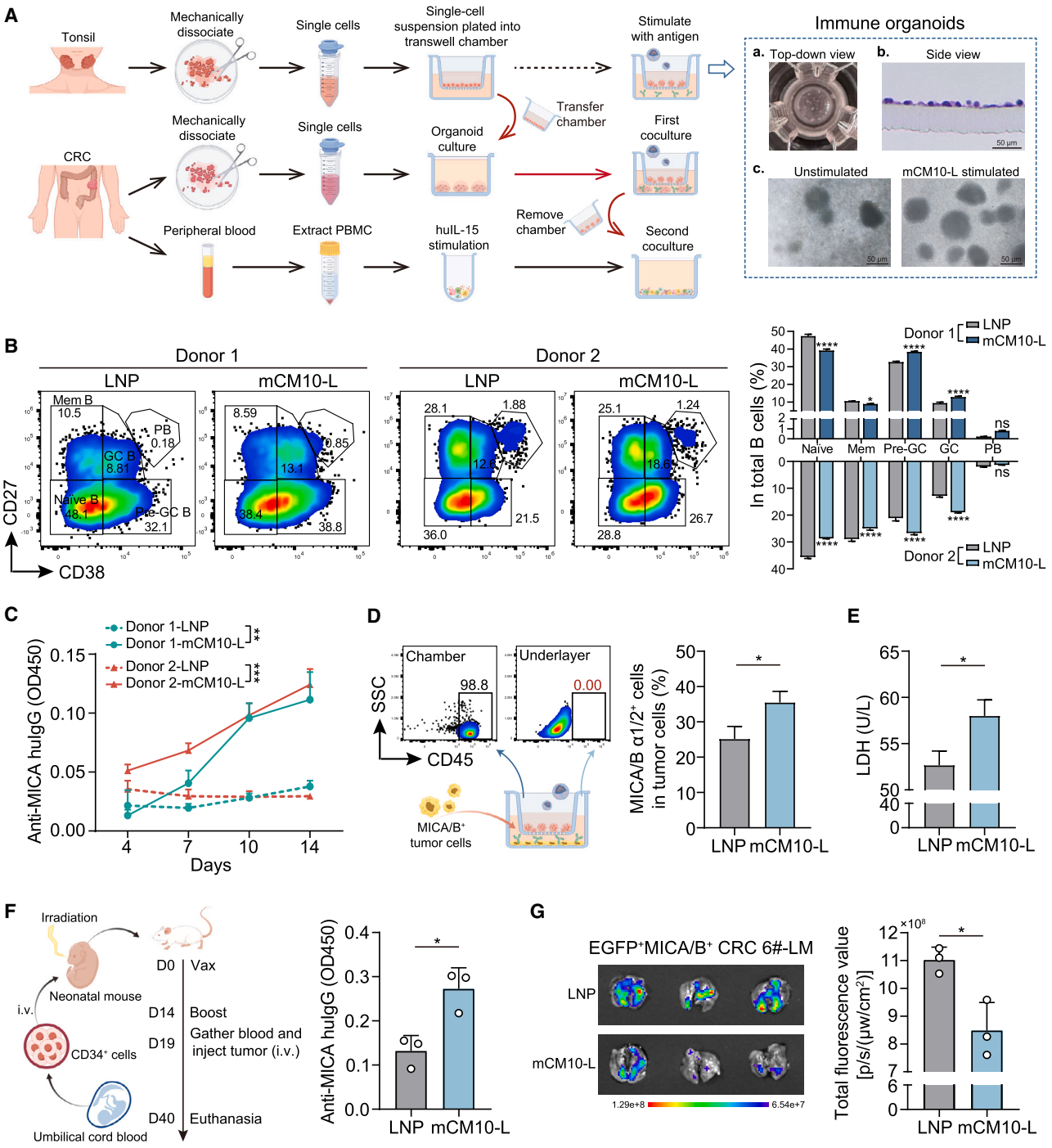

Figure 6. mCM10-L elicited a specific B cell antitumor response in human immune cell-based models

(A) Workflow of an *in vitro* immune organoid-colorectal cancer organoid-PBMC interaction model (left) and representative images of immune organoids (right). The top-down view was photographed (a), the side view was displayed under light microscopy post H&E staining (b), and the reaggregation degree of immune cells after mCM10-L stimulation (0.5 μg/well) was observed under light microscopy (c). Scale bar, 50 μm (b) and 50 μm (c). $n = 3$ independent experiments.

(B and C) mCM10-L was added to immune organoids (0.5 μg/well) and cultured for 14 days, with an equal dose of LNPs as a control. Representative (left) and quantification (right) of FCM for B cell differentiation under mCM10-L stimulation (B). Naive B: naive B cells ($CD27^-CD38^-$); Mem B: memory B cells ($CD27^+CD38^-$); Pre-GC B: pre-germinal center B cells ($CD27^-CD38^+$); GC B: germinal center B cells ($CD27^+CD38^+$); PB: plasmablasts ($CD27^+CD38^{+++}$). The concentration of anti-MICA hulgG antibody secreted in the medium was measured by ELISA (C). $n = 3$ independent experiments.

(legend continued on next page)

with this observation, our study revealed that MICA/B α1/2 shedding occurs in CRC and becomes more severe in patients with metastasis. The metastatic potential of tumor cells was greatly increased when the α1/2 domain was absent from the membrane surface, suggesting that MICA/B hydrolysis might be closely related to latency before tumor metastasis. Therefore, long-lasting and preventive immune monitoring of the random shedding of MICA/B α1/2 achieved through tumor vaccines is a feasible approach for eradicating LCC cells in a timely manner and preventing tumor metastasis and is highly important for improving the prognosis of patients with cancer.

In contrast to the neoantigens of personalized tumor vaccines, MICA/B, the target of Ma3P-related vaccines, is a broad-spectrum tumor antigen, and the amino acid sequence of Ma3P is conserved across the most prevalent MICA alleles. Moreover, Ma3P-related vaccines rely mainly on a B cell epitope, which directly binds to the corresponding B cell receptor in the B cell repertoire to activate humoral immune responses, independent of the tumor mutation burden or MHC restriction.[37–40] The activation of robust B cell immunity requires auxiliary signals from helper T cells.[41] Our study revealed that Ma3P does not possess definite mouse $CD4^+$ T/$CD8^+$ T cell epitopes but can still produce specific antibodies through the identified B cell epitope with Quil A adjuvant to exert antimetastatic effects. Notably, MICA/B is expressed at low levels as an autoantigen in human bladder, bronchial, kidney, and colon epithelial cells and is upregulated in the intestinal epithelium of patients with Crohn's disease, *E. coli* infection, or *Mycobacterium tuberculosis* infection, as well as in the bronchial epithelium of patients with allergies or viral infections.[42–45] Despite successful treatment of cancer with chimeric antigen receptor (CAR)-T/CAR-NK cells targeting MICA/B α3 in mice, whether T cell-mediated killing by targeting MICA/B α3 causes severe autoimmune responses needs further clinical validation.[3] Since bioinformatics analysis and our experiments revealed that Ma3P also contains several human HLA allele-binding epitopes, such side effects should be considered as well. In conclusion, Ma3P is a dominant sequence that deserves further optimization for the advanced development of combined or multivalent vaccines.

Adjuvants are essential for improving the quality and magnitude of adaptive immune responses to vaccines. Quil A, which expands the antibody repertoire and enhances the antibody titer, was selected as an adjuvant for Ma3P vaccination in mice.[46] However, clinical options for adjuvants are fairly limited owing to the severe cytotoxicity accompanying nonspecific immune activation.[47] The exploitation of mRNA-LNPs has greatly accelerated the development of vaccines. After mRNAs are encapsulated in stable LNPs with adjuvant activity, they directly enter the cytoplasm to act as antigens and induce strong cellular and humoral responses without infectivity or integration; moreover, they are degraded by physiological cellular processes soon after injection.[25,26,48] Therefore, we switched to Ma3P in the form of mRNA-LNPs and shifted the vaccination method from subcutaneous injection, which results in the quick absorption of antigens, thus preventing degradation, to the more commonly used intramuscular injection, to enable the fast recognition and processing of antigens by the immune system, resulting in rapid immune responses. To improve the efficacy of vaccines, CRM197 has been widely used as a carrier protein for antigens to combat a variety of infectious diseases and breast cancer with the purpose of increasing immunogenicity.[49,50] Indeed, our study revealed that mCM10-L, encoding CRM197 with 10 Ma3P repeats, induced the production of specific antibodies that blocked MICA/B α1/2 shedding, whereas mM1-L did not. Additionally, mCM10-L had strong antimetastatic effects comparable to those of mCa3-L and ma3-L, reflecting the feasibility of our strategy for designing B cell epitope-based vaccines; however, whether the specificity of induced antibodies increases and whether their safety in humans is improved need further exploration. Notably, we found that the proportion of MDSCs from lung tissues with metastatic tumors was increased in mCM10-L-vaccinated mice showed by CyTOF, indicating that further combined inhibition of MDSCs may improve mCM10-L efficacy.

Mice with a competent immune system are the preferred model for validating vaccine efficacy in preclinical studies. In our study, multiple metastasis models were used, such as a tumor dissemination model, which was established via tumor cell tail vein injection, and a spontaneous metastasis model, which was established via orthotopic tumor inoculation followed by resection. However, animal models remain limited due to differences in immune responses caused by species distinctions. Immune organoids constructed from human tonsils can partially recapitulate the complexities of the human adaptive immune system and have been used to evaluate B cell-based vaccines.[51–53] We found that a bit of mRNA-LNPs were present in macrophages and dendritic cells, whereas almost all mRNA-LNPs were absorbed by B cells, $CD4^+$ T/$CD8^+$ T cells, and plasma cells, which may be related to the proportion of immune organoid cells. As expected, mCM10-L exhibited excellent immunogenicity in human immune organoids by promoting B cell differentiation and inducing the production of anti-MICA

(D) Contactless coculture system of human immune organoids with MICA/B^+ HCT116 cells (left). mCM10-L was added to immune organoids (0.5 μg/well) and cultured for 10 days, with an equal dose of LNPs as a control. The level of MICA/B α1/2 on the membrane of tumor cells was evaluated by FCM (right). $n = 3$ independent experiments.

(E) Immune organoids stimulated with mCM10-L (0.5 μg/well) or the LNPs control for 14 days were contactlessly cocultured with CRC organoids for an additional 24 h. The CRC organoids were subsequently retrieved and cocultured with matched PBMCs at a 1:20 ratio for 4 to 6 h. The content of LDH released into the medium was measured via spectrophotometry. $n = 3$ independent experiments.

(F and G) mCM10-L (3 μg/100 μL) was injected intramuscularly into HSC-humanized C-NKG mice ($n = 3$ per group) on days 0 and 14, with an equal dose of LNPs as a control. Serum was collected 5 days post second immunization, and the level of specific anti-MICA huIgG antibody in the serum (diluted 1:5) was measured by ELISA (F). EGFP$^+$MICA/B^+ CRC 6#-LM cells were then injected into vaccinated mice via the tail vein. Following experimental termination, the lungs were collected, and the tumor burden, expressed as the total fluorescence value (Ex:480 nm/Em:520 nm), was assessed (G).

Data are presented as the mean ± SDs and were analyzed by two-way ANOVA (B) or unpaired Student's t test (C–G). ns: no significant difference, $^*p < 0.05$, $^{**}p < 0.01$, $^{***}p < 0.001$, and $^{****}p < 0.0001$. See also Figure S6.

huIgG antibody, which blocked MICA/B α1/2 shedding. Unlike the response to exogenous viral infections, endogenous tumor antigens are tolerated by the modified immune system of patients with tumor during long-term adaptive evolution.[54] Immune organoids alone cannot be used to predict whether the antibodies elicited by vaccines can disrupt immune tolerance and activate the antitumor response.[55] Thus, we established an *in vitro* human immune organoid-CRC organoid-PBMC interaction model, which allows the specific antibodies secreted by human immune organoids to act fully on the tumor organoids and then come into direct contact with PBMCs isolated from the corresponding patients with tumor. The results indicated that mCM10-L could promote MICA/B-mediated antitumor immunity in humans and that this interaction model was effective for the prediction of antitumor activity triggered by B cell vaccines.

In summary, our mRNA vaccine based on the identified B cell epitope from the MICA α3 proteolytic region induced the production of specific antibodies and thus activated antitumor immunity in various models, with promising application prospects for preventing and inhibiting MICA/B$^+$ tumor metastasis.

Limitations of the study

In this study, we designed an antigenic peptide with a focus on the B cell epitope from the MICA α3 proteolytic region. After elongation to both ends of the identified epitope and confirmation of its immunogenicity, the amino acid sequence of Ma3P was not further optimized or modified. To predict the immunoreactivity of mCM10-L in humans, we constructed an *in-vitro*-interacting human organoid model, which partially filled the gap regarding appropriate models to evaluate antitumor activity. However, several limitations remain: (1) samples obtained after routine tonsillectomy were prone to age bias (most were from young children); (2) most of the tonsil samples exhibited chronic low-grade inflammation; (3) the cell composition of immune organoids prepared from tonsils was inconsistent with the immune microenvironment at the vaccination site; and (4) the samples prepared for interactions between immune organoids and tumor organoids were not obtained from the same patient, possibly leading to heterologous immune activation. Thus, we propose that pathologically negative lymph nodes resected from patients with tumors during surgery may be used to prepare immune organoids to address the aforementioned shortcomings.

RESOURCE AVAILABILITY

Lead contact

Further information and requests for resources and reagents should be directed to and will be fulfilled by the lead contact, Yongliang Zhu (ylzhu@zju.edu.cn).

Materials availability

All plasmids and reagents generated in this study are available from the lead contact with a completed Materials Transfer Agreement.

Data and code availability

- All data reported in this paper will be shared by the lead contact upon request. This paper does not report original code.
- Any additional information required to reanalyze the data reported in this paper is available from the lead contact upon request.

ACKNOWLEDGMENTS

We would like to thank Prof. Hongxiang Sun (College of Animal Sciences, Zhejiang University) for research guidance on animal adjuvants. Thanks to Dr. Ming Chen and Dr. Lei Shen (Department of Otorhinolaryngology, the Second Affiliated Hospital of Zhejiang University School of Medicine) for collecting tonsil samples. Thanks to Qinghua Lv (Key Laboratory of Cancer Prevention and Intervention, the Second Affiliated Hospital of Zhejiang University School of Medicine) for helpful technical support in FCM. This work was supported by the National Key R&D Program of China (2022YFA1105200), the National Natural Science Foundation of China (82173350, 81872407, and 82002950), and the Key R&D Program of Zhejiang Province (2020C03013). The cartoons shown in the graphical abstract and figures were generated with BioRender and Figdraw 2.0.

AUTHOR CONTRIBUTIONS

Conceptualization, R.W. and Y.Z.; methodology, R.W., J.W., Y.L., Y.X., B.Y., S.Y., Z.F., and S.L.; investigation, R.W. and J.W.; visualization, R.W. and Y.L.; funding acquisition, T.P. and Y.Z.; project administration, C.W. and Y.Z.; supervision, C.W. and Y.Z.; writing – original draft, R.W.; writing – review and editing, R.W., Y.L., and Y.Z.

DECLARATION OF INTERESTS

The authors declare no competing interests.

STAR★METHODS

Detailed methods are provided in the online version of this paper and include the following:

- KEY RESOURCES TABLE
- EXPERIMENTAL MODEL AND STUDY PARTICIPANT DETAILS
  - Human samples
  - Cell lines and cell culture
  - Mice
- METHOD DETAILS
  - Preparation of primary human colorectal cancer cells
  - Construction of overexpressing cell lines via lentiviral transduction
  - Plasmid construction
  - Expression of recombinant proteins
  - Preparation of anti-MICA/B antibodies
  - Immunofluorescence staining
  - *In vitro* detection for the inhibition of MICA/B α1/2 shedding
  - ELISA
  - Validation of identified epitopes
  - Production of vaccines
  - Subcutaneous tumor models
  - Lung metastasis models
  - Spontaneous metastasis models after surgical removal of primary tumors
  - *In vivo* depletion of mouse immune cells
  - Isolation of mouse immune cells
  - Isolation of human PBMCs
  - *In vitro* cytotoxicity assay
  - FCM
  - CyTOF
  - Immune organoid culture
  - Colorectal cancer organoid culture
  - Immune organoid–tumor organoid–PBMC interaction model
- QUANTIFICATION AND STATISTICAL ANALYSIS

SUPPLEMENTAL INFORMATION

Supplemental information can be found online at https://doi.org/10.1016/j.xcrm.2025.101981.

CellPress
OPEN ACCESS

Received: May 4, 2024
Revised: November 27, 2024
Accepted: January 28, 2025
Published: February 24, 2025

REFERENCES

1. Steeg, P.S. (2006). Tumor metastasis: mechanistic insights and clinical challenges. Nat. Med. *12*, 895–904. https://doi.org/10.1038/nm1469.
2. Valastyan, S., and Weinberg, R.A. (2011). Tumor metastasis: molecular insights and evolving paradigms. Cell *147*, 275–292. https://doi.org/10.1016/j.cell.2011.09.024.
3. Goulding, J., Yeh, W.I., Hancock, B., Blum, R., Xu, T., Yang, B.H., Chang, C.W., Groff, B., Avramis, E., Pribadi, M., et al. (2023). A chimeric antigen receptor uniquely recognizing MICA/B stress proteins provides an effective approach to target solid tumors. Med *4*, 457–477.e8. https://doi.org/10.1016/j.medj.2023.04.004.
4. Espinoza, I., Agarwal, S., Sakiyama, M., Shenoy, V., Orr, W.S., Diffalha, S.A., Prizment, A., Varambally, S., Manne, U., and Gomez, C.R. (2021). Expression of MHC class I polypeptide-related sequence A (MICA) in colorectal cancer. Front. Biosci. *26*, 765–776. https://doi.org/10.52586/4986.
5. Fang, L., Gong, J., Wang, Y., Liu, R., Li, Z., Wang, Z., Zhang, Y., Zhang, C., Song, C., Yang, A., et al. (2014). MICA/B expression is inhibited by unfolded protein response and associated with poor prognosis in human hepatocellular carcinoma. J. Exp. Clin. Cancer Res. *33*, 76. https://doi.org/10.1186/s13046-014-0076-7.
6. Hayakawa, Y., Kelly, J.M., Westwood, J.A., Darcy, P.K., Diefenbach, A., Raulet, D., and Smyth, M.J. (2002). Cutting edge: tumor rejection mediated by NKG2D receptor-ligand interaction is dependent upon perforin. J. Immunol. *169*, 5377–5381. https://doi.org/10.4049/jimmunol.169.10.5377.
7. Kaiser, B.K., Yim, D., Chow, I.T., Gonzalez, S., Dai, Z., Mann, H.H., Strong, R.K., Groh, V., and Spies, T. (2007). Disulphide-isomerase-enabled shedding of tumour-associated NKG2D ligands. Nature *447*, 482–486. https://doi.org/10.1038/nature05768.
8. Boukouaci, W., Busson, M., Peffault de Latour, R., Rocha, V., Suberbielle, C., Bengoufa, D., Dulphy, N., Haas, P., Scieux, C., Amroun, H., et al. (2009). MICA-129 genotype, soluble MICA, and anti-MICA antibodies as biomarkers of chronic graft-versus-host disease. Blood *114*, 5216–5224. https://doi.org/10.1182/blood-2009-04-217430.
9. Kohga, K., Takehara, T., Tatsumi, T., Miyagi, T., Ishida, H., Ohkawa, K., Kanto, T., Hiramatsu, N., and Hayashi, N. (2009). Anticancer chemotherapy inhibits MHC class I-related chain a ectodomain shedding by downregulating ADAM10 expression in hepatocellular carcinoma. Cancer Res. *69*, 8050–8057. https://doi.org/10.1158/0008-5472.CAN-09-0789.
10. Ashiru, O., Boutet, P., Fernández-Messina, L., Agüera-González, S., Skepper, J.N., Valés-Gómez, M., and Reyburn, H.T. (2010). Natural killer cell cytotoxicity is suppressed by exposure to the human NKG2D ligand MICA*008 that is shed by tumor cells in exosomes. Cancer Res. *70*, 481–489. https://doi.org/10.1158/0008-5472.CAN-09-1688.
11. Ferrari de Andrade, L., Tay, R.E., Pan, D., Luoma, A.M., Ito, Y., Badrinath, S., Tsoucas, D., Franz, B., May, K.F., Jr., Harvey, C.J., et al. (2018). Antibody-mediated inhibition of MICA and MICB shedding promotes NK cell-driven tumor immunity. Science *359*, 1537–1542. https://doi.org/10.1126/science.aao0505.
12. Du, C., Bevers, J., 3rd, Cook, R., Lombana, T.N., Rajasekaran, K., Matsumoto, M., Spiess, C., Kim, J.M., and Ye, Z. (2019). MICA immune complex formed with alpha 3 domain-specific antibody activates human NK cells in a Fc-dependent manner. J. Immunother. Cancer *7*, 207. https://doi.org/10.1186/s40425-019-0687-9.
13. Ferrari de Andrade, L., Kumar, S., Luoma, A.M., Ito, Y., Alves da Silva, P.H., Pan, D., Pyrdol, J.W., Yoon, C.H., and Wucherpfennig, K.W. (2020). Inhibition of MICA and MICB shedding elicits NK-cell-mediated immunity against tumors resistant to cytotoxic T cells. Cancer Immunol. Res. *8*, 769–780. https://doi.org/10.1158/2326-6066.Cir-19-0483.
14. Alves da Silva, P.H., Xing, S., Kotini, A.G., Papapetrou, E.P., Song, X., Wucherpfennig, K.W., Mascarenhas, J., and Ferrari de Andrade, L. (2022). MICA/B antibody induces macrophage-mediated immunity against acute myeloid leukemia. Blood *139*, 205–216. https://doi.org/10.1182/blood.2021011619.
15. Courau, T., Bonnereau, J., Chicoteau, J., Bottois, H., Remark, R., Assante Miranda, L., Toubert, A., Blery, M., Aparicio, T., Allez, M., and Le Bourhis, L. (2019). Cocultures of human colorectal tumor spheroids with immune cells reveal the therapeutic potential of MICA/B and NKG2A targeting for cancer treatment. J. Immunother. Cancer *7*, 74. https://doi.org/10.1186/s40425-019-0553-9.
16. Kennedy, L.B., and Salama, A.K.S. (2020). A review of cancer immunotherapy toxicity. CA. Cancer J. Clin. *70*, 86–104. https://doi.org/10.3322/caac.21596.
17. Zhang, Y., and Zhang, Z. (2020). The history and advances in cancer immunotherapy: understanding the characteristics of tumor-infiltrating immune cells and their therapeutic implications. Cell. Mol. Immunol. *17*, 807–821. https://doi.org/10.1038/s41423-020-0488-6.
18. Peng, M., Mo, Y., Wang, Y., Wu, P., Zhang, Y., Xiong, F., Guo, C., Wu, X., Li, Y., Li, X., et al. (2019). Neoantigen vaccine: an emerging tumor immunotherapy. Mol. Cancer *18*, 128. https://doi.org/10.1186/s12943-019-1055-6.
19. Torres, N., Regge, M.V., Secchiari, F., Friedrich, A.D., Spallanzani, R.G., Raffo Iraolagoitia, X.L., Núñez, S.Y., Sierra, J.M., Ziblat, A., Santilli, M.C., et al. (2020). Restoration of antitumor immunity through anti-MICA antibodies elicited with a chimeric protein. J. Immunother. Cancer *8*, e000233. https://doi.org/10.1136/jitc-2019-000233.
20. Badrinath, S., Dellacherie, M.O., Li, A., Zheng, S., Zhang, X., Sobral, M., Pyrdol, J.W., Smith, K.L., Lu, Y., Haag, S., et al. (2022). A vaccine targeting resistant tumours by dual T cell plus NK cell attack. Nature *606*, 992–998. https://doi.org/10.1038/s41586-022-04772-4.
21. Cecil, D.L., Holt, G.E., Park, K.H., Gad, E., Rastetter, L., Childs, J., Higgins, D., and Disis, M.L. (2014). Elimination of IL-10-inducing T-helper epitopes from an IGFBP-2 vaccine ensures potent antitumor activity. Cancer Res. *74*, 2710–2718. https://doi.org/10.1158/0008-5472.CAN-13-3286.
22. Zhong, S., Liu, Z., Zhou, Y., Zhang, T., Fu, X., Guo, L., Gu, S., Tang, L., Hou, J., and Li, Y. (2022). Longitudinal mapping of hepatitis B vaccine-induced B-cell linear epitopes in healthy individuals. J. Med. Virol. *94*, 4993–5006. https://doi.org/10.1002/jmv.27926.
23. Kratochvil, S., Shen, C.H., Lin, Y.C., Xu, K., Nair, U., Da Silva Pereira, L., Tripathi, P., Arnold, J., Chuang, G.Y., Melzi, E., et al. (2021). Vaccination in a humanized mouse model elicits highly protective PfCSP-targeting anti-malarial antibodies. Immunity *54*, 2859–2876.e7. https://doi.org/10.1016/j.immuni.2021.10.017.
24. Hamley, I.W. (2022). Peptides for vaccine development. ACS Appl. Bio Mater. *5*, 905–944. https://doi.org/10.1021/acsabm.1c01238.
25. Qin, S., Tang, X., Chen, Y., Chen, K., Fan, N., Xiao, W., Zheng, Q., Li, G., Teng, Y., Wu, M., and Song, X. (2022). mRNA-based therapeutics: powerful and versatile tools to combat diseases. Signal Transduct. Target. Ther. *7*, 166. https://doi.org/10.1038/s41392-022-01007-w.
26. Gebre, M.S., Brito, L.A., Tostanoski, L.H., Edwards, D.K., Carfi, A., and Barouch, D.H. (2021). Novel approaches for vaccine development. Cell *184*, 1589–1603. https://doi.org/10.1016/j.cell.2021.02.030.
27. Sahin, U., Karikó, K., and Türeci, Ö. (2014). mRNA-based therapeutics—developing a new class of drugs. Nat. Rev. Drug Discov. *13*, 759–780. https://doi.org/10.1038/nrd4278.
28. Zong, Y., Lin, Y., Wei, T., and Cheng, Q. (2023). Lipid nanoparticle (LNP) enables mRNA delivery for cancer therapy. Adv. Mater. *35*, e2303261. https://doi.org/10.1002/adma.202303261.
29. Ortega-Rivera, O.A., Shin, M.D., Chen, A., Beiss, V., Moreno-Gonzalez, M.A., Lopez-Ramirez, M.A., Reynoso, M., Wang, H., Hurst, B.L., Wang,

J., et al. (2021). Trivalent subunit vaccine candidates for COVID-19 and their delivery devices. J. Am. Chem. Soc. *143*, 14748–14765. https://doi.org/10.1021/jacs.1c06600.

30. Ma, Z., Mao, C., Chen, X., Yang, S., Qiu, Z., Yu, B., Jia, Y., Wu, C., Wang, Y., Wang, Y., et al. (2023). Peptide vaccine against ADAMTS-7 ameliorates atherosclerosis and postinjury neointima hyperplasia. Circulation *147*, 728–742. https://doi.org/10.1161/CIRCULATIONAHA.122.061516.
31. Schoen, R.E., Boardman, L.A., Cruz-Correa, M., Bansal, A., Kastenberg, D., Hur, C., Dzubinski, L., Kaufman, S.F., Rodriguez, L.M., Richmond, E., et al. (2023). Randomized, double-blind, placebo-controlled trial of MUC1 peptide vaccine for prevention of recurrent colorectal adenoma. Clin. Cancer Res. *29*, 1678–1688. https://doi.org/10.1158/1078-0432.CCR-22-3168.
32. Wiedermann, U., Garner-Spitzer, E., Chao, Y., Maglakelidze, M., Bulat, I., Dechaphunkul, A., Arpornwirat, W., Charoentum, C., Yen, C.J., Yau, T.C., et al. (2021). Clinical and immunologic responses to a B-cell epitope vaccine in patients with HER2/neu-overexpressing advanced gastric cancer-results from Phase Ib Trial IMU.ACS.001. Clin. Cancer Res. *27*, 3649–3660. https://doi.org/10.1158/1078-0432.CCR-20-3742.
33. Barsoum, I.B., Hamilton, T.K., Li, X., Cotechini, T., Miles, E.A., Siemens, D.R., and Graham, C.H. (2011). Hypoxia induces escape from innate immunity in cancer cells via increased expression of ADAM10: role of nitric oxide. Cancer Res. *71*, 7433–7441. https://doi.org/10.1158/0008-5472.CAN-11-2104.
34. Wang, B., Wang, Q., Wang, Z., Jiang, J., Yu, S.C., Ping, Y.F., Yang, J., Xu, S.L., Ye, X.Z., Xu, C., et al. (2014). Metastatic consequences of immune escape from NK cell cytotoxicity by human breast cancer stem cells. Cancer Res. *74*, 5746–5757. https://doi.org/10.1158/0008-5472.CAN-13-2563.
35. Massague, J., and Obenauf, A.C. (2016). Metastatic colonization by circulating tumour cells. Nature *529*, 298–306. https://doi.org/10.1038/nature17038.
36. Malladi, S., Macalinao, D.G., Jin, X., He, L., Basnet, H., Zou, Y., de Stanchina, E., and Massagué, J. (2016). Metastatic latency and immune evasion through autocrine inhibition of WNT. Cell *165*, 45–60. https://doi.org/10.1016/j.cell.2016.02.025.
37. Havenar-Daughton, C., Abbott, R.K., Schief, W.R., and Crotty, S. (2018). When designing vaccines, consider the starting material: the human B cell repertoire. Curr. Opin. Immunol. *53*, 209–216. https://doi.org/10.1016/j.coi.2018.08.002.
38. Melief, C.J.M., van Hall, T., Arens, R., Ossendorp, F., and van der Burg, S.H. (2015). Therapeutic cancer vaccines. J. Clin. Investig. *125*, 3401–3412. https://doi.org/10.1172/JCI80009.
39. Sahin, U., and Türeci, Ö. (2018). Personalized vaccines for cancer immunotherapy. Science *359*, 1355–1360. https://doi.org/10.1126/science.aar7112.
40. Yu, Z., Liu, W., He, Y., Sun, M., Yu, J., Jiao, X., Han, Q., Tang, H., Zhang, B., Xian, Y., et al. (2021). HLA-A2.1-restricted ECM1-derived epitope LA through DC cross-activation priming CD8(+) T and NK cells: a novel therapeutic tumour vaccine. J. Hematol. Oncol. *14*, 71. https://doi.org/10.1186/s13045-021-01081-7.
41. Cyster, J.G., and Allen, C.D.C. (2019). B cell responses: cell interaction dynamics and decisions. Cell *177*, 524–540. https://doi.org/10.1016/j.cell.2019.03.016.
42. Ghadially, H., Brown, L., Lloyd, C., Lewis, L., Lewis, A., Dillon, J., Sainson, R., Jovanovic, J., Tigue, N.J., Bannister, D., et al. (2017). MHC class I chain-related protein A and B (MICA and MICB) are predominantly expressed intracellularly in tumour and normal tissue. Br. J. Cancer *116*, 1208–1217. https://doi.org/10.1038/bjc.2017.79.
43. Perera, L., Shao, L., Patel, A., Evans, K., Meresse, B., Blumberg, R., Geraghty, D., Groh, V., Spies, T., Jabri, B., and Mayer, L. (2007). Expression of nonclassical class I molecules by intestinal epithelial cells. Inflamm. Bowel Dis. *13*, 298–307. https://doi.org/10.1002/ibd.20026.
44. Tieng, V., Le Bouguénec, C., du Merle, L., Bertheau, P., Desreumaux, P., Janin, A., Charron, D., and Toubert, A. (2002). Binding of *Escherichia coli* adhesin AfaE to CD55 triggers cell-surface expression of the MHC class I-related molecule MICA. Proc. Natl. Acad. Sci. USA *99*, 2977–2982. https://doi.org/10.1073/pnas.032668099.
45. Borchers, M.T., Harris, N.L., Wesselkamper, S.C., Vitucci, M., and Cosman, D. (2006). NKG2D ligands are expressed on stressed human airway epithelial cells. Am. J. Physiol. Lung Cell. Mol. Physiol. *291*, L222–L231. https://doi.org/10.1152/ajplung.00327.2005.
46. Orbegozo-Medina, R.A., Martínez-Sernández, V., González-Warleta, M., Castro-Hermida, J.A., Mezo, M., and Ubeira, F.M. (2018). Vaccination of sheep with Quil-A® adjuvant expands the antibody repertoire to the *Fasciola* MF6p/FhHDM-1 antigen and administered together impair the growth and antigen release of flukes. Vaccine *36*, 1949–1957. https://doi.org/10.1016/j.vaccine.2018.02.115.
47. Sun, H.X., Xie, Y., and Ye, Y.P. (2009). Advances in saponin-based adjuvants. Vaccine *27*, 1787–1796. https://doi.org/10.1016/j.vaccine.2009.01.091.
48. Chen, J., Ye, Z., Huang, C., Qiu, M., Song, D., Li, Y., and Xu, Q. (2022). Lipid nanoparticle-mediated lymph node-targeting delivery of mRNA cancer vaccine elicits robust CD8(+) T cell response. Proc. Natl. Acad. Sci. USA *119*, e2207841119. https://doi.org/10.1073/pnas.2207841119.
49. Chen, S., Quan, D.H., Sam, G., Ozberk, V., Wang, X.T., Halfmann, P., Pandey, M., Good, M.F., Kawaoka, Y., Britton, W.J., and Rehm, B.H.A. (2023). Assembly of immunogenic protein particles toward advanced synthetic vaccines. Small *19*, e2205819. https://doi.org/10.1002/smll.202205819.
50. Tobias, J., Jasinska, J., Baier, K., Kundi, M., Ede, N., Zielinski, C., and Wiedermann, U. (2017). Enhanced and long term immunogenicity of a Her-2/neu multi-epitope vaccine conjugated to the carrier CRM197 in conjunction with the adjuvant Montanide. BMC Cancer *17*, 118. https://doi.org/10.1186/s12885-017-3098-7.
51. Wagar, L.E., Salahudeen, A., Constantz, C.M., Wendel, B.S., Lyons, M.M., Mallajosyula, V., Jatt, L.P., Adamska, J.Z., Blum, L.K., Gupta, N., et al. (2021). Modeling human adaptive immune responses with tonsil organoids. Nat. Med. *27*, 125–135. https://doi.org/10.1038/s41591-020-01145-0.
52. Kastenschmidt, J.M., Sureshchandra, S., Jain, A., Hernandez-Davies, J.E., de Assis, R., Wagoner, Z.W., Sorn, A.M., Mitul, M.T., Benchorin, A.I., Levendosky, E., et al. (2023). Influenza vaccine format mediates distinct cellular and antibody responses in human immune organoids. Immunity *56*, 1910–1926.e7. https://doi.org/10.1016/j.immuni.2023.06.019.
53. Yin, Q., Luo, W., Mallajosyula, V., Bo, Y., Guo, J., Xie, J., Sun, M., Verma, R., Li, C., Constantz, C.M., et al. (2023). A TLR7-nanoparticle adjuvant promotes a broad immune response against heterologous strains of influenza and SARS-CoV-2. Nat. Mater. *22*, 380–390. https://doi.org/10.1038/s41563-022-01464-2.
54. Kim, T.K., Vandsemb, E.N., Herbst, R.S., and Chen, L. (2022). Adaptive immune resistance at the tumour site: mechanisms and therapeutic opportunities. Nat. Rev. Drug Discov. *21*, 529–540. https://doi.org/10.1038/s41573-022-00493-5.
55. Morrocchi, E., van Haren, S., Palma, P., and Levy, O. (2024). Modeling human immune responses to vaccination *in vitro*. Trends Immunol. *45*, 32–47. https://doi.org/10.1016/j.it.2023.11.002.
56. Qiu, Y., Yang, S., Pan, T., Yu, L., Liu, J., Zhu, Y., and Wang, H. (2019). ANKRD22 is involved in the progression of prostate cancer. Oncol. Lett. *18*, 4106–4113. https://doi.org/10.3892/ol.2019.10738.
57. Liu, J., Wu, J., Wang, R., Zhong, D., Qiu, Y., Wang, H., Song, Z., and Zhu, Y. (2021). ANKRD22 drives rapid proliferation of Lgr5(+) cells and acts as a promising therapeutic target in gastric mucosal injury. Cell. Mol. Gastroenterol. Hepatol. *12*, 1433–1455. https://doi.org/10.1016/j.jcmgh.2021.06.020.
58. Han, G., Spitzer, M.H., Bendall, S.C., Fantl, W.J., and Nolan, G.P. (2018). Metal-isotope-tagged monoclonal antibodies for high-dimensional mass cytometry. Nat. Protoc. *13*, 2121–2148. https://doi.org/10.1038/s41596-018-0016-7.

STAR★METHODS

KEY RESOURCES TABLE

REAGENT or RESOURCE	SOURCE	IDENTIFIER
Antibodies		
Peroxidase-conjugated AffiniPure goat anti-mouse IgG (H + L)	Jackson ImmunoResearch	Cat# 115-035-003, RRID: AB_10015289
Peroxidase-conjugated AffiniPure F(ab')2 fragment goat anti-mouse IgM	Jackson ImmunoResearch	Cat# 115-036-020, RRID: AB_2338521
Peroxidase-conjugated AffiniPure goat anti-human IgG (H + L)	Jackson ImmunoResearch	Cat# 109-035-003, RRID: AB_2337577
R-phycoerythrin-conjugated AffiniPure F(ab')2 fragment goat anti-mouse IgG	Jackson ImmunoResearch	Cat# 115-116-071, RRID: AB_2338626
Recombinant anti-β actin antibody (Mouse)	Servicebio	Cat# GB15001, RRID: AB_3083704
Anti-human MICA/B α3 antibody (Mouse, Clone: MIA-2)	This paper	N/A
Anti-human MICA/B α1/2 antibody (Mouse, Clone: MIA-16)	This paper	N/A
Anti-human MICA/B α1/2 antibody (Mouse, Clone: MIA-18)	This paper	N/A
InVivoMab anti-mouse CD4 (Clone: GK1.5)	BioXcell	Cat# BE0003, RRID: AB_1107642
InVivoMab anti-mouse CD8a (Clone: 2.43)	BioXcell	Cat# BE0061, RRID: AB_1125541
InVivoMab anti-mouse NK1.1 (Clone: PK136)	BioXcell	Cat# BE0036, RRID: AB_1107737
InVivoMab anti-mouse B220 (Clone: RA3.3A1/6.1 (TIB-146))	BioXcell	Cat# BE0067, RRID: AB_1107651
APC anti-human MICA/B (Clone: 6D4)	BioLegend	Cat# 320907, RRID: AB_493196
FITC anti-human CD326 (EpCAM) (Clone: 9C4)	BioLegend	Cat# 324203, RRID: AB_756077
PE/Cyanine 7 anti-mouse CD45 (Clone: 30-F11)	BioLegend	Cat# 103114, RRID: AB_312979
APC/Cyanine7 anti-mouse CD4 (Clone: RM4-5)	BioLegend	Cat# 100526, RRID: AB_312727
Alexa Fluor® 700 anti-mouse CD3 (Clone: 17A2)	BioLegend	Cat# 100216, RRID: AB_493697
PerCP/Cyanine5.5 anti-mouse CD8a (Clone: 53-6.7)	BioLegend	Cat# 100734, RRID: AB_2075238
APC anti-mouse NK1.1 (Clone: PK136)	BD Pharmingen	Cat# 550627, RRID: AB_398463
PE-CF594 anti-mouse IFN-γ (Clone: XMG1.2)	BD Pharmingen	Cat# 562303, RRID: AB_11153140
Brilliant Violet 421™ anti-human/mouse Granzyme B (Clone: QA18A28)	BioLegend	Cat# 396414, RRID: AB_2810603
FITC anti-human CD45 (Clone: HI30)	BioLegend	Cat# 982316, RRID: AB_2876779
APC anti-human CD19 (Clone: HIB19)	BioLegend	Cat# 982406, RRID: AB_2650645
PerCP/Cyanine5.5 anti-human CD45 (Clone: HI30)	BioLegend	Cat# 304028, RRID: AB_893338
Brilliant Violet 605™ anti-human CD3 (Clone: UCHT1)	BioLegend	Cat# 300459, RRID: AB_2564379
FITC anti-human CD4 (Clone: SK3)	BioLegend	Cat# 344604, RRID: AB_1937227
APC/Cyanine7 anti-human CD8 (Clone: SK1)	BioLegend	Cat# 344714, RRID: AB_2044006
APC anti-human IFN-γ (Clone: 4S.B3)	BioLegend	Cat# 502512, RRID: AB_315237

(*Continued on next page*)

Continued

REAGENT or RESOURCE	SOURCE	IDENTIFIER
PerCP/Cyanine5.5 anti-mouse CD19 (Clone: 6D5)	BioLegend	Cat# 115534, RRID: AB_2072925
Brilliant Violet 421™ anti-mouse IgD (Clone: 11-26c.2a)	BioLegend	Cat# 405725, RRID: AB_2562743
Brilliant Violet 605™ anti-mouse CD138 (Syndecan-1) (Clone: 281-2)	BioLegend	Cat# 142531, RRID: AB_2715767
APC anti-mouse CD73 (Clone: TY/11.8)	BioLegend	Cat# 127209, RRID: AB_11219400
PE anti-mouse CD80 (Clone: 16-10A1)	BioLegend	Cat# 104707, RRID: AB_313128
APC/Cyanine7 anti-mouse IgM (Clone: RMM-1)	BioLegend	Cat# 406515, RRID: AB_10690815
Brilliant Violet 421™ anti-human TCRγ/δ (Clone: B1)	BioLegend	Cat# 331217, RRID: AB_2562316
PE/Cyanine 7 anti-human CD4 (Clone: SK3)	BioLegend	Cat# 344611, RRID: AB_2028477
PE anti-human CD56 (Clone: QA17A16)	BioLegend	Cat# 985902, RRID: AB_2910522
PE/Dazzle™ 594 anti-human CD138 (Syndecan-1) (Clone: DL-101)	BioLegend	Cat# 352320, RRID: AB_2687342
PE anti-human CD11b (Clone: ICRF44)	BioLegend	Cat# 982606, RRID: AB_2650641
APC/Cyanine7 anti-human HLA-DR (Clone: L243)	BioLegend	Cat# 307618, RRID: AB_493586
Brilliant Violet 605™ anti-human CD123 (Clone: 6H6)	BioLegend	Cat# 306025, RRID: AB_2562115
PE/Cyanine 7 anti-human CD68 (Clone: Y1/82A)	BioLegend	Cat# 333816, RRID: AB_2562936
Brilliant Violet 421™ anti-human CD14 (Clone: 63D3)	BioLegend	Cat# 367143, RRID: AB_2810579
PE/Cyanine 7 anti-human CD45 (Clone: HI30)	BioLegend	Cat# 982310, RRID: AB_2715773
APC anti-human CD3 (Clone: UCHT1)	BioLegend	Cat# 300412, RRID: AB_314066
PerCP/Cyanine5.5 anti-human CD19 (Clone: HIB19)	BioLegend	Cat# 982412, RRID: AB_2820226
PE anti-mouse/rat/human CD27 (Clone: LG.3A10)	BioLegend	Cat# 124209, RRID: AB_1236464
FITC anti-human CD38 (Clone: HB-7)	BioLegend	Cat# 356609, RRID: AB_2561949
Bacterial and virus strains		
E. coli BL21(DE3) cells	Novagen	Cat# 69450-M
Biological samples		
Colorectal cancer tissues, tonsil tissues, and peripheral blood samples	See experimental model and study participant details	See Tables S1 and S2
Chemicals, peptides, and recombinant proteins		
Hyaluronidase	Sigma-Aldrich	Cat# H3631
Type IV collagenase	Sigma-Aldrich	Cat# C5138
Matrigel (Growth factor reduced)	Corning	Cat# 356230
IntestiCult™ OGM Human Basal Medium	Stemcell	Cat# 100-0190
Fetal bovine serum	ExCell Bio	Cat# FSP500
Penicillin–streptomycin	Cienry	Cat# CR15140
QuickCut™ BamHI	Takara	Cat# 1605
QuickCut™ HindIII	Takara	Cat# 1615
QuickCut™ EcoRI	Takara	Cat# 1611
QuickCut™ DpnI	Takara	Cat# 1609
T4 ligase	Takara	Cat# 2011A
Isopropyl-β-D-thiogalactopyranoside	Sangon Biotech	Cat# A600168

(*Continued on next page*)

Continued

REAGENT or RESOURCE	SOURCE	IDENTIFIER
Lysozyme	Sangon Biotech	Cat# A610308
Recombinant human MICA protein (C-6His)	Novoprotein	Cat# C489
Horseradish peroxidase-labeled streptavidin	Beyotime	Cat# A0305
Lipofectamine™ 3000	Invitrogen	Cat# L3000015
D-luciferin potassium salt	Yeasen	Cat# 40902ES03
Ficoll-Hypaque separation solution	TBD	Cat# LTS1077
Recombinant human IL-2	Novoprotein	Cat# C013
ACK lysis buffer	Beyotime	Cat# C3702
BV510-Zombie Dye	BioLegend	Cat# 423102
Fixation Buffer	BioLegend	Cat# 420801
Intracellular Staining Perm Wash Buffer	BioLegend	Cat# 421002
Cisplatin	Fluidigm	Cat# 201064
Maxpar Fix and Perm Buffer	Fluidigm	Cat# 201067
Ir	Fluidigm	Cat# 201192A
Perm buffer	eBioscience	Cat# 00-8333-56
EQ beads	Fluidigm	Cat# 201078
Nonessential amino acids	Gibco	Cat# 11140050
Sodium pyruvate	Gibco	Cat# 11360070
Insulin/selenium/transferrin cocktail	Procell	Cat# PB180429
Recombinant human BAFF (carrier-free)	BioLegend	Cat# 559602
Tumor tissue digestion solution	bioGenous	Cat# K601003
Cancer organoid basal medium	bioGenous	Cat# B213152
Colorectal cancer organoid complete medium	bioGenous	Cat# K2103-CR
Recombinant human IL-15	Novoprotein	Cat# C016
Cell Activation Cocktail with Brefeldin A	BioLegend	Cat# 423303
Brefeldin A	BioLegend	Cat# 420601
MojoSort™ Buffer	BioLegend	Cat# 480017
Critical commercial assays		
MojoSort™ Mouse CD8 T cell Isolation Kit	BioLegend	Cat# 480007
MojoSort™ Mouse NK Cell Isolation Kit	BioLegend	Cat# 480049
Annexin V-Elab Fluor647®/PI Apoptosis Kit	Procell	Cat# P-CA-203
Experimental models: Cell lines		
Mus: MC38	BMCR	Cat# 1101MOU-PUMC000523
Mus: B16-F10	ATCC	Cat# CRL-6475
Mus: 4T1	ATCC	Cat# CRL-2539
Homo: HCT116	ATCC	Cat# CCL-247
Homo: A375	ATCC	Cat# CRL-1619
Homo: HEK293T	ATCC	Cat# CRL-3216
Experimental models: Organisms/strains		
Mouse: C57BL/6	Shanghai SLAC Laboratory Animal Co.	N/A
Mouse: BALB/c	Shanghai SLAC Laboratory Animal Co.	N/A
Mouse: M-NSG	Shanghai Model Organisms Center	Cat# C001316
Mouse: huPBMC-C-NKG	Cyagen Bio	Cat# C001329
Mouse: huHSC-C-NKG-ProF	Cyagen Bio	Cat# C001543
Oligonucleotides		
Primers used, see Table S3	Sangon Biotech	N/A

(*Continued on next page*)

Continued

REAGENT or RESOURCE	SOURCE	IDENTIFIER
Recombinant DNA		
EGFP-tagged *MICA* (allele 001)-overexpressing recombinant lentiviral vector	Cyagen Biosciences	N/A
EGFP-tagged $MICA^{\Delta\alpha1/2}$ ($\alpha1-\alpha2$ domain deletion)-overexpressing recombinant lentiviral vector	Cyagen Biosciences	N/A
MICA-pCMV6-XL5 (allele 001) mammalian expression plasmid	OriGene	Cat# sc120030
MICA $\alpha3$-pUC57 *E coli* cloning plasmid	OriGene	N/A
Software and algorithms		
GraphPad Prism 9.0 software	GraphPad Software, Inc.	https://graphpad.com/scientificsoftware/prism/
FlowJo 10.8	Tree Star Inc.	https://www.flowjo.com/solutions/flowjo
ImageJ	NIH	https://imagej.net/ij
Aniview	BLT	https://www.blt-imaging.com/
Other		
Website: IEDB	NIAID	https://www.iedb.org
Website: SWISS-MODEL	N/A	https://swissmodel.expasy.org
Website: NetMHCIIpan-4.0	DTU Health Tech	https://services.healthtech.dtu.dk/services/NetMHCIIpan-4.0/
Website: NetMHC-4.0	DTU Health Tech	https://services.healthtech.dtu.dk/services/NetMHC-4.0/
Database: IPD-IMGT/HLA	N/A	https://www.ebi.ac.uk/ipd/imgt/hla/

EXPERIMENTAL MODEL AND STUDY PARTICIPANT DETAILS

Human samples

Fresh tumor tissues from 4 patients with CRC (Case ID: P4, JMH 5#, CRC 6#-LM and CRC 16#) using for the preparation of primary colorectal cancer cells were obtained from the Second Affiliated Hospital of Zhejiang University School of Medicine. The patients had not received any anticancer therapy before surgical resection. Informed consent was obtained from all participants, and the experimental protocol was approved by the Clinical Research Ethics Committee of the Second Affiliated Hospital of Zhejiang University School of Medicine (2019LSYD072H). Sample information is listed in Table S1.

Fresh tumor tissues from 9 patients with CRC using for FCM, paraffin sections from 10 patients with CRC using for immunofluorescence staining, serum from 55 patients with CRC and 5 healthy donors using for ELISA or incubating cells, fresh peripheral blood from 12 healthy donors using for the isolation of PBMCs, fresh tumor tissue and matched peripheral blood from 1 patient with CRC using for the construction of tumor organoids, and fresh tonsil tissues from 2 patients using for the construction of immune organoids were all obtained from the Second Affiliated Hospital of Zhejiang University School of Medicine. CRC patients were pathologically diagnosed and had not received any anticancer therapy before the samples were collected. The patients who underwent tonsillectomy were surgically treated for obstructive sleep apnea or chronic tonsillitis. Informed consent was obtained from all participants, and the experimental protocol was approved by the Clinical Research Ethics Committee of the Second Affiliated Hospital of Zhejiang University School of Medicine (2019LSYD072H and 2024LSYD0966H). Sample information is listed in Table S2.

This study was carried out in accordance with the principles of the Declaration of Helsinki.

Cell lines and cell culture

Mouse colon adenocarcinoma MC38, human melanoma A375 and human HEK293T cells were cultured in DMEM (Corning, 10-013-CV) supplemented with 10% fetal bovine serum (FBS; ExCell Bio, FSP500) and 1× penicillin–streptomycin (Cienry, CR15140). Mouse melanoma B16-F10, mouse breast cancer 4T1 and human colon cancer HCT116 cells were cultured in RPMI 1640 medium (Corning, 10-040-CV) supplemented with 10% FBS and 1× penicillin–streptomycin. These cells were cultured at 37°C in the presence of 5% carbon dioxide (CO_2).

Mice

All the animal studies were approved by the Animal Ethics Committee of the Second Affiliated Hospital of Zhejiang University School of Medicine (2022NDD207H). Female 6-8-week-old C57BL/6 mice and female 6-8-week-old BALB/c mice were purchased from

Shanghai SLAC Laboratory Animal Co., Ltd. Female 6-8-week-old M-NSG mice were purchased from Shanghai Model Organisms Center, Inc. Female 9-week-old PBMC-humanized C-NKG mice and female 13-week-old HSC-humanized C-NKG mice were purchased from Cyagen Bio. All the mice were housed under specific pathogen-free (SPF) conditions in ventilated cages under a 12-h light/dark cycle at a constant temperature and humidity, with access to water and food *ad libitum*.

METHOD DETAILS

Preparation of primary human colorectal cancer cells

Fresh human CRC tissues were digested with 0.5 mg/mL hyaluronidase (Sigma-Aldrich, H3631) and 1 mg/mL type IV collagenase (Sigma-Aldrich, C5138) at 37°C for 80 min, after which the resulting cell pellets were resuspended in Matrigel (Corning, 356230) at a 1:4 ratio and cultured in organoid medium (Stemcell, 100–0190) for 7 to 14 days. The culture medium was changed every 2 days. For xenotransplantation, harvested organoids were subcutaneously inoculated into M-NSG mice. After tumor formation, the subcutaneous tumors were retrieved and digested into single-cell suspensions. These primary cells were then cultured in DMEM/F12 (Corning, 10-092-CVRC) supplemented with 10% FBS and 1× penicillin–streptomycin for further use.

Construction of overexpressing cell lines via lentiviral transduction

The EGFP-tagged *MICA* (allele 001)-overexpressing recombinant lentiviral vector and EGFP-tagged *MICA*$^{\Delta\alpha1/2}$ ($\alpha1-\alpha2$ domain deletion)-overexpressing recombinant lentiviral vector with corresponding lentiviruses were constructed by Cyagen Biosciences. Cell transfection with these lentiviruses was performed in accordance with the manufacturer's instructions. Then, 5 μg/mL polybrene was added to increase transfection efficiency. After 48 to 72 h of incubation, EGFP^{+} cells were isolated via fluorescence-activated cell sorting (FACS) and successful transfection was verify by FCM.

Plasmid construction

The *MICA*-pCMV6-XL5 (allele 001) mammalian expression plasmid was purchased from OriGene (sc120030). The *MICA* $\alpha3$-pUC57 *E coli* cloning plasmid was synthesized by OriGene.

To construct the plasmids for the expression of truncated MICA $\alpha3$ mutants T1-T4 in *E. coli*, *MICA* $\alpha3$-pUC57 was used as a template, and the target gene fragments were cloned and inserted into the pET42a vector after PCR amplification and double digestion with BamHI (Takara, 1605) and HindIII (Takara, 1615) endonucleases.

To construct the plasmids for the expression of spliced MICA $\alpha3$ mutants D1-D8 in *E. coli*, the *MICA* $\alpha3$ fragment was first subcloned from the pUC57 vector into the pET32a vector and then used as a template, and the target plasmid was synthesized via PCR amplification, EcoRI (Takara, 1611) and DpnI (Takara, 1609) endonucleases digestion and T4 ligase (Takara, 2011A) ligation.

To construct the plasmid for the expression of MICA$^{\Delta SHDTQQ}$ (SHDTQQ sequence deletion) in HEK293T cells. *MICA*-pCMV6-XL5 was used as a template, and the target plasmid was synthesized via PCR amplification, BamHI and DpnI endonucleases digestion and T4 ligase ligation.

The primers were chemically synthesized by Sangon Biotech and are listed in Table S3.

Expression of recombinant proteins

MICA/B $\alpha3$ and its mutants were expressed via the *E. coli* system as previously described.[56] In brief, the plasmids were transformed into *E. coli* BL21(DE3) cells (Novagen, 69450-M). The expression of the recombinant proteins was induced in liquid LB medium containing 0.5 mmol/L isopropyl-β-D-thiogalactopyranoside (Sangon Biotech, A600168), and the cells were lysed with 100 μg/mL lysozyme (Sangon Biotech, A610308) and sonicated (30 cycles of sonication at 90 W for 10 s in an ice bath) to obtain inclusion bodies (IBs). The IB pellets were dissolved in dissolution buffer (50 mL of dissolution buffer consisting of 5 mL of 10× IB solubilization buffer, 0.5 mL of 30% N-lauroylsarcosine, 50 μL of 1 M dithiothreitol (DTT) and 44.45 mL of deionized water) and subjected to refolding by redox dialysis. Finally, the recombinant proteins were purified on a Ni^{2+} column (Bio-Rad Laboratories) and their purity and size were confirmed by SDS–PAGE.

Preparation of anti-MICA/B antibodies

Anti-MICA/B antibodies were prepared via the traditional hybridoma method. In brief, recombinant human MICA protein (Novoprotein, C489) was used as an immunogen to immunize BALB/c mice via subcutaneous injection. Mouse splenocytes were collected and fused to SP2/0 cells at a 10:1 ratio to generate hybridoma cells. After limiting dilution cloning, the positive clones bound to MICA/B on the cell membrane surface were identified by FCM, and their binding to the recombinant MICA $\alpha3$ protein was evaluated by ELISA. These hybridoma cells were fed and expanded in the peritoneal cavity of mice, and the ascites fluid was collected and purified to obtain the corresponding high-purity murine monoclonal IgG antibodies. Via the above steps, the MIA-2 clone targeting MICA/B $\alpha3$ and the MIA-16/18 clones targeting MICA/B $\alpha1/2$ were obtained. Further humanized modification of MIA-2 was performed by SanyouBio.

Immunofluorescence staining

Sections of paraffin-embedded CRC tissues were incubated with an anti-MICA/B $\alpha3$ antibody (clone: MIA-2, diluted 1:1000) plus an anti-MICA/B $\alpha1/2$ antibody (clone: MIA-16, diluted 1:1000), and then visualized with AF488-TSA (diluted 1:1000, Servicebio, G1222)

plus AF594-TSA (diluted 1:2000, Servicebio, G1223). The cell nuclei were counterstained with DAPI (Servicebio, G1012). Immunofluorescence images were captured using a Nikon digital sight DS-FI2 (NIKON Eclipse ci) and the area percentage of fluorescence in each channel was measured by ImageJ.

In vitro detection for the inhibition of MICA/B α1/2 shedding

A375 cells (with endogenous MICA/B expression) were cultured in 48-well plates. MIA-2 or the sterile mouse serum (diluted 1:8) was added to the medium. After incubation overnight, the culture supernatants were collected and centrifuged, and the concentration of sMICA/B was measured by ELISA. A375 cells were then retrieved by treating with 0.02% EDTA (without trypsin), and the surface expression of MICA/B α1/2 was evaluated via FCM.

ELISA

To identify the epitope recognized by MIA-2, recombinant MICA α3 and related mutant proteins, as well as BSA conjugates with SHDTQQW, were diluted to 20 μg/mL with CBS buffer (pH 9.6, 1.59 g of Na_2CO_3 and 2.93 g of $NaHCO_3$ dissolved in 1 L of deionized water) and added to the 96-well ELISA plates (JET BIOFIL, FEP101896) (100 μL/well) at 4°C overnight. After blocking with 10% FBS, 100 μL of 10 μg/mL MIA-2 was added to each well and incubated at 37°C for 1 h. After washing 5 times with 1× TBST buffer, peroxidase-conjugated AffiniPure goat anti-mouse IgG (H + L) (diluted 1:4000, Jackson ImmunoResearch, 115-035-003) was added and incubated at 37°C for 1 h. After another 5 washes, 3,3′,5,5′-tetramethylbenzidine (TMB) dihydrochloride was added and allowed to react at room temperature for 10 min. The absorbance at 450 nm was measured with a microplate reader (Molecular Devices, USA) after termination with stop solution. For the peptide blocking experiment, 20 μg/mL recombinant MICA α3 was precoated on plates at 100 μL/well overnight. 10 μg/mL MIA-2 was premixed 1:1 with 250 μg/mL peptide (PEP1-PEP4) at 37°C for 1 h, and then the mixture was added to the plates at 100 μL/well. The other steps were performed as described above.

To measure the concentration of anti-MICA antibodies in the serum, ELISA plates were precoated with 5 μg/mL recombinant human MICA protein at 4°C overnight. After being blocked with 10% FBS, the samples were diluted appropriately and then added to the plates at 100 μL/well for incubation. After washing, peroxidase-conjugated AffiniPure goat anti-mouse IgG (H + L) (diluted 1:4000), peroxidase-conjugated AffiniPure F(ab')2 fragment goat anti-mouse IgM (diluted 1:4000, Jackson ImmunoResearch, 115-036-020) or peroxidase-conjugated AffiniPure goat anti-human IgG (H + L) (diluted 1:4000, Jackson ImmunoResearch, 109-035-003) was added. The other steps were performed as described above.

To measure the concentration of sMICA/B in the serum and culture supernatants, ELISA plates were precoated with 25 μg/mL anti-MICA/B α1/2 antibody (clone: MIA-16) overnight. After blocking, the test samples were diluted appropriately and then added to the plates at 100 μL/well for incubation. After washing, 1 μg/mL biotin-conjugated anti-MICA/B α1/2 antibody (clone: MIA-18) was added (100 μL/well), and the plates were incubated at 37°C for 1 h. After another wash, horseradish peroxidase-labeled streptavidin (diluted 1:4000, Beyotime, A0305) was added. The other steps were performed as described above.

Validation of identified epitopes

HEK293T cells were cultured in 6-well plates and transfected with the *MICA*-pCMV6-XL5 and $MICA^{\Delta SHDTQQ}$-pCMV6-XL5 plasmids using Lipofectamine 3000 (Invitrogen, L3000015) according to the manufacturer's instructions. After incubation for 48 h, the cells were treated with 0.02% EDTA and then collected.

For linear epitope identification, the cell pellets were treated with ice-cold radioimmunoprecipitation assay (RIPA) lysis buffer for 30 min to extract total protein, and Western blot analysis was then performed as previously described.[57] The membranes containing the linear $MICA^{Full\text{-}length}$ and $MICA^{\Delta SHDTQQ}$ proteins were incubated with MIA-2 (1 mg/mL, diluted 1:1000) at 4°C overnight, with an anti-MICA/B α1/2 antibody (clone: MIA-16, 1 mg/mL, diluted 1:1000) as a positive control and an anti-β-actin antibody (diluted 1:1000, Servicebio, GB15001) as a loading control. After washing with 1× TBST buffer, peroxidase-conjugated AffiniPure goat anti-mouse IgG (H + L) (diluted 1:3000) was added, and the mixture was incubated at room temperature for 1 h. All the membranes were imaged via a Tannon 5200.

For steric epitope identification, the cell suspensions were incubated with 100, 10, 1 or 0.1 μg/mL MIA-2 at 4°C for 30 min, with an APC-conjugated anti-MICA/B α1/2 antibody (BioLegend, 320907) as a positive control. After washing with PBS, R-phycoerythrin-conjugated AffiniPure F(ab')2 fragment goat anti-mouse IgG (diluted 1:500, Jackson ImmunoResearch, 115-116-071) was added, and the mixture was incubated at 4°C for 30 min prior to analysis by FCM.

Production of vaccines

For Ma3P, the peptide was synthesized by QYAOBIO, and its purity and molecular weight were determined via high-performance liquid chromatography (HPLC) and mass spectrometry (MS).

For mCM10-L, mM1-L, mCa3-L and ma3-L, the corresponding mRNAs were codon optimized, sequenced, synthesized and encapsulated in LNPs by ProMab Bio. The LNPs used were lipid mixtures containing the ethanol phase of SM-102, DSPC, cholesterol and DMG-PEG2000 (at a molar % ratio of 50:10:38.5:1.5). After mixing LNPs with an aqueous solution of mRNA in 100 mM sodium acetate (pH 4.0) at a flow rate ratio of 1:3 (organic: aqueous) and purifying, the encapsulation rate of these mRNA-LNPs was greater than 95%.

Subcutaneous tumor models

To detect MICA/B α1/2 shedding from the tumor cell surface *in vivo*, PBMC-humanized C-NKG mice were inoculated subcutaneously with MICA/B$^+$ P4 cells (100 μL, 4×10^6 cells per mouse) on day 0. Sacrifice was performed on day 15, and the subcutaneous tumors were then harvested for FCM analysis.

To evaluate the antitumor effect of huMIA-2, PBMC-humanized C-NKG mice were inoculated subcutaneously with MICA/B$^+$ JMH 5#, CRC 6#-LM or CRC 16# cells (100 μL, 4×10^6 cells per mouse) on day 0. HuMIA-2 or the isotype control was injected intraperitoneally (200 μg per mouse) on days −1, 0, 5, 7 and 10. Sacrifice was performed on day 15, and the subcutaneous tumors were then harvested, photographed and weighed.

Lung metastasis models

To investigate the relationship between MICA/B α1/2 on the surface of tumor cells and metastasis, C57BL/6 mice were inoculated with EGFP$^+$MICA$^+$ MC38 cells or EGFP$^+$MICA$^{\Delta\alpha1/2+}$ MC38 cells (100 μL, 9×10^5 cells per mouse) via the tail vein on day 0. Sacrifice was performed on day 25, and the lungs were then harvested and subjected to fluorescence imaging.

To evaluate the antimetastatic effect of MIA-2, C57BL/6 mice were inoculated with EGFP$^+$MICA$^+$ MC38 cells (100 μL, 9×10^5 cells per mouse) or EGFP$^+$MICA$^+$ B16-F10 cells (100 μL, 3.5×10^5 cells per mouse) via the tail vein on day 0. MIA-2 or the isotype control was injected intraperitoneally (200 μg per mouse) on days −1, 0, 5, 7 and 10. Sacrifice was performed on day 25, and the lungs were then harvested, photographed or subjected to fluorescence imaging.

To evaluate the ability of vaccines to prevent tumor metastasis, Ma3P (100 μL, 20 μg per mouse) was mixed with Quil A (100 μL, 7.5 μg per mouse) and then injected subcutaneously into the inner thighs of C57BL/6 mice on days 0 and 14, with an equal volume of PBS mixed with Quil A as a control. mCM10-L, mCa3-L or ma3-L (100 μL, 3 μg per mouse) was injected intramuscularly into the outer thighs of C57BL/6 mice on days 0 and 14, with an equal dose of LNPs as a control. Five days after the second immunization, peripheral blood was collected, and specific anti-MICA antibodies were detected by ELISA. The mice were further inoculated with EGFP$^+$MICA$^+$ MC38 cells (100 μL, 9×10^5 cells per mouse) or EGFP$^+$MICA$^+$ B16-F10 cells (100 μL, 3.5×10^5 cells per mouse) via the tail vein. All the mice were euthanized on day 44, and the lungs were then harvested, photographed or subjected to fluorescence imaging. For predicting the ability of mCM10-L to prevent tumor metastasis in humans, mCM10-L (100 μL, 3 μg per mouse) was injected intramuscularly into HSC-humanized C-NKG mice on days 0 and 14, with an equal dose of LNPs as a control. After detection for serum antibodies, the mice were inoculated with EGFP$^+$MICA/B$^+$ CRC 6#-LM cells (100 μL, 1×10^6 cells per mouse) via the tail vein. Sacrifice was performed on day 40, and the lungs were then harvested and subjected to fluorescence imaging.

To evaluate the effects of vaccines in treating metastatic tumors, C57BL/6 mice were inoculated with EGFP$^+$MICA$^+$ MC38 cells (100 μL, 9×10^5 cells per mouse) via the tail vein on day 0. mCM10-L (100 μL, 3 μg per mouse) was then injected intramuscularly into the mice on days 5 and 14 after tumorigenesis, with an equal dose of LNPs as a control. All the mice were euthanized on day 25, and the lungs were then harvested and subjected to fluorescence imaging.

Spontaneous metastasis models after surgical removal of primary tumors

Luciferase$^+$MICA$^+$ 4T1 cells (100 μL, 4×10^6 cells per mouse) were injected into the fat pads of BALB/c mice. The tumors were surgically removed on day 25 when the volume reached about 250–300 mm^3. mCM10-L (100 μL, 3 μg per mouse) was then injected intramuscularly into the outer thighs of the mice one day post operation, with an equal dose of LNPs as a control. A booster was administered 14 days later. D-luciferin potassium salt (150 mg/kg, Yeasen, 40902ES03) was injected intraperitoneally into the mice and *in vivo* bioluminescence imaging was performed under anesthesia every 7 days after surgery to track tumor recurrence and metastasis.

In vivo depletion of mouse immune cells

Anti-CD4 antibody (αCD4, BioXcell, BE0003), anti-CD8a antibody (αCD8a, BioXcell, BE0061) or anti-NK1.1 antibody (αNK1.1, BioXcell, BE0036) was injected intraperitoneally at 200 μg/100 μL per mouse once every 3 days, starting at the described time points to deplete CD4$^+$ T cells, CD8$^+$ T cells or NK cells *in vivo,* respectively. Anti-B220 antibody (αB220, BioXcell, BE0067) was injected intraperitoneally at 200 μg/100 μL per mouse once every 2 weeks, starting at the described time point to deplete B cells *in vivo*.

Isolation of mouse immune cells

CD8$^+$ T cells and NK cells from mouse peripheral blood were isolated with a MojoSort Mouse CD8 T cell Isolation Kit (BioLegend, 480007) and a MojoSort Mouse NK Cell Isolation Kit (BioLegend, 480049), respectively, according to the manufacturer's instructions. In brief, 100 μL of the cell suspension (10^7 cells) was transferred to a 5 mL tube and 10 μL of Biotin-Antibody Cocktail was added. The mixture was incubated on ice for 15 min, followed by adding 10 μL of Streptavidin nanobeads and incubating on ice for another 15 min, and then resuspended in 2.5 mL of MojoSort Buffer (BioLegend, 480017). Place the tube in a magnet for 5 min, and the sorted cells was poured out and collected.

Isolation of human PBMCs

Fresh peripheral blood from healthy donors was collected in tubes with EDTA-Na_2. PBMCs were isolated with Ficoll-Hypaque separation solution (TBD, LTS1077) according to the manufacturer's instructions. Briefly, the separation solution was added to a 15 mL

centrifuge tube. The blood was diluted with PBS and carefully spread over the separation solution at a 1:1:1 ratio. The samples were horizontally centrifuged at 2000 rpm at room temperature for 20 min with an acceleration of 2 and a deceleration of 1. The cells in the intermediate layer were pipetted into a new centrifuge tube, and the PBMCs were collected.

In vitro cytotoxicity assay

To determine the role of MICA/B α1/2 in immune activation, PBMCs prestimulated with 1000 U/mL huIL-2 (Novoprotein, C013) overnight were cocultured with $EGFP^+MICA^+$ or -$EGFP^+MICA^{\Delta\alpha1/2+}$ HCT116 cells at a 10:1 ratio for 4 to 6 h.

To evaluate the role of MIA-2 in immune activation, $EGFP^+MICA^+$ HCT116 cells were preincubated with 10 μg/mL huMIA-2 or the isotype control overnight and then cocultured with prestimulated PBMCs at a 1:10 ratio for 4 to 6 h.

To verify the activities of effector cells from mouse peripheral blood, isolated $CD8^+$ T cells or NK cells were counted and cocultured with MC38 cells at a 1:20 ratio for 12 h.

The culture supernatants were collected for determination of the LDH content via spectrophotometry and the IFN-γ concentration by FCM. The cells were stained with an Annexin V-Elab Fluor647/PI Apoptosis Kit (Procell, P-CA-203) according to the manufacturer's instructions to evaluate apoptosis in $EGFP^+$ tumor cells by FCM.

FCM

The tumors and lungs were cut into small pieces with surgical scissors to avoid the use of digestive enzymes that affect MICA/B α1/2 detection. Mice spleens were pulverized, and peripheral blood was treated with ACK lysis buffer (Beyotime, C3702) at room temperature for 10 min. These samples were then filtered through 70-μm cell strainers to prepare single-cell suspensions. BV510-Zombie Dye (diluted 1:500, BioLegend, 423102) was added to all the samples for live-cell staining. For surface staining, the cells were mixed with fluorochrome-conjugated antibodies at 4°C for 30 min to label the surface markers. For intracellular staining, the cells were first incubated with Cell Activation Cocktail (with BFA) (BioLegend, 423303) or BFA (BioLegend, 420601) at 37°C in the presence of 5% CO_2 for 6 h, fixed with Fixation Buffer (BioLegend, 420801) at room temperature for 20 min, permeabilized with 1× Intracellular Staining Perm Wash Buffer (BioLegend, 421002) at room temperature for another 20 min, and finally stained with fluorochrome-conjugated antibodies at 4°C for 50 min to label the intracellular markers.

The following antibody panel was designed to analyze tumor cells: FITC-huEpCAM (BioLegend, 324203) (used for tumor cells without EGFP expression), MIA-2 (50 μg/mL) and APC-huMICA/B (BioLegend, 320907). The cells were washed in 1× PBS and further stained with R-phycoerythrin-conjugated AffiniPure F(ab')2 Fragment Goat Anti-Mouse IgG (diluted 1:500) at 4°C for 30 min to fluorescently label MIA-2.

The following antibody panel was designed to analyze the cytotoxic activity of mouse immune cells: PE/Cyanine 7-mCD45 (BioLegend, 103114), Alexa Fluor 700-mCD3 (BioLegend, 100216), APC/Cyanine7-mCD4 (BioLegend, 100526), PerCP/Cyanine5.5-mCD8a (BioLegend, 100734), APC-mNK1.1 (BD Pharmingen, 550627), PE-CF594-mIFN-γ (BD Pharmingen, 562303) and Brilliant Violet 421-mGranzyme B (BioLegend, 396414).

The following antibody panel was designed to analyze the degree of humanization in mice: PE/Cyanine 7-mCD45, FITC-huCD45 (BioLegend, 982316) and APC-huCD19 (BioLegend, 982406).

The following antibody panel was designed to analyze the cytotoxic activity of human immune cells: PerCP/Cyanine5.5-huCD45 (BioLegend, 304028), Brilliant Violet 605-huCD3 (BioLegend, 300459), FITC-huCD4 (BioLegend, 344604), APC/Cyanine7-huCD8 (BioLegend, 344714) and APC-huIFN-γ (BioLegend, 502512).

The following antibody panel was designed to analyze the memory B cells in mice spleens: PE/Cyanine 7-mCD45, PerCP/Cyanine5.5-mCD19 (BioLegend, 115534), Brilliant Violet 421-mIgD (BioLegend, 405725), Brilliant Violet 605-mCD138 (BioLegend, 142531), APC-mCD73 (BioLegend, 127209), PE-mCD80 (BioLegend, 104707) and APC/Cyanine7-mIgM (BioLegend, 406515).

The following antibody panel was designed to analyze human lymphoid cells: PerCP/Cyanine5.5-huCD45, Brilliant Violet 605-huCD3, Brilliant Violet 421-huTCRγ/δ (BioLegend, 331217), PE/Cyanine 7-huCD4 (BioLegend, 344611), APC/Cyanine7-huCD8, PE-huCD56 (BioLegend, 985902), APC-huCD19 and PE/Dazzle 594-huCD138 (BioLegend, 352320).

The following antibody panel was designed to analyze human myeloid cells: PerCP/Cyanine5.5-huCD45, PE-huCD11b (BioLegend, 982606), APC/Cyanine7-huHLA-DR (BioLegend, 307618), Brilliant Violet 605-huCD123 (BioLegend, 306025), PE/Cyanine 7-huCD68 (BioLegend, 333816) and Brilliant Violet 421-huCD14 (BioLegend, 367143).

The following antibody panel was designed to analyze B-cell differentiation in human immune organoids: PE/Cyanine 7-huCD45 (BioLegend, 982310), APC-huCD3 (BioLegend, 300412), PerCP/Cyanine5.5-huCD19 (BioLegend, 982412), PE-huCD27 (BioLegend, 124209) and FITC-huCD38 (BioLegend, 356609).

The above samples were examined with a DxFLEX flow cytometer (Beckman Coulter, USA), and the data were then analyzed with FlowJo software (Tree Star, Inc.).

CyTOF

CyTOF analysis of immune cells infiltrated in mice lungs with metastatic tumors was performed by PLTTech, Inc. following a previously published protocol.[58] In brief, the samples were washed once in 1× PBS and first stained with 250 nM cisplatin (Fluidigm, 201064) on ice for 5 min. Cells were blocked with FcR, stained with an in-house-developed panel of surface antibodies on ice for 30 min, and then fixed in intercalation solution (Maxpar Fix and Perm Buffer (Fluidigm, 201067) containing 250 nM 191/193Ir

(Fluidigm, 201192A)) overnight. After another round of washing, the cells were then permeabilized in perm buffer (eBioscience, 00-8333-56) and stained with a panel of intracellular antibodies on ice for 30 min. Prior to signals acquisition on a mass spectrometry cytometer (Helios, Fluidigm), the cells were resuspended in deionized water with additional 20% EQ beads (Fluidigm, 201078). All the markers and their corresponding labels are listed in Table S4.

For analysis, data from each sample were debarcoded from raw data using a doublet-filtering scheme with unique mass-tagged barcodes. Each.fcs file was normalized by the bead normalization method. Manually gating data using FlowJo software to exclude debris, dead cells, and adhesions. Apply the Phenograph clustering algorithm to all cells to classify cells into different phenotypes based on marker expression levels. Annotate the cell type of each cluster based on the label expression pattern on the cluster vs. marker heatmap. The dimensionality reduction algorithm t-SNE was used to visualize data in two dimensions and showed the distribution of each cluster and distinct marker expression among each group.

Immune organoid culture

Immune organoids were constructed post preparation and cryopreservation of tonsil cells as previously described.[51] Briefly, after thawing, the dissociated tonsil cells were resuspended at 5×10^7 cells/mL in complete medium (RPMI 1640 medium, 10% FBS, 1× penicillin–streptomycin, 1× nonessential amino acids (Gibco, 11140050), 1× sodium pyruvate (Gibco, 11360070) and 1× insulin/selenium/transferrin cocktail (Procell, PB180429)) and plated on permeable (0.4-μm pore size) membranes (polycarbonate membranes in standard 24-well plates, Corning, 3413) at 100 μL/well with no matrix support. To each well, 1 mL of complete medium containing 0.5 μg/mL huBAFF (BioLegend, 559602) was added, and the culture medium was replaced with 30% fresh medium every 3 to 4 days mCM10-L (0.5 μg/well) was directly added to the chambers on day 0, with an equal dose of LNPs as a control. Immune organoids were reaggregated and formed by culture under humidified conditions at 37°C in 5% CO_2 for 10 to 14 days. The cells in the chambers were used for analysis of B-cell differentiation and the supernatants underlay were used for detection of antibody levels.

Colorectal cancer organoid culture

The tumor tissues were rinsed 5 times in basic DMEM containing 1× penicillin–streptomycin, fully minced, and then digested in tumor tissue digestion solution (bioGenous, K601003) at 37°C for 60 min. After the addition of FBS to terminate digestion, the suspensions were filtered through 70-μm cell strainers. The cells were washed once in cancer organoid basal medium (bioGenous, B213152) and resuspended in Matrigel (Corning, 356230). The mixtures were pipetted in the wells, and the plates were inverted and incubated at 37°C in a 5% CO_2 incubator for 20 min. After the Matrigel solidified, colorectal cancer organoid complete medium (bioGenous, K2103-CR) was slowly added. The organoids were cultured at 37°C in the presence of 5% CO_2, and the medium was changed every 2 days.

Immune organoid–tumor organoid–PBMC interaction model

To construct the interaction model of human immune organoid–tumor organoid–PBMC, chambers containing structured immune organoids which have been cultured for 14 days were first transferred over the wells containing Matrigel-encapsulated 3D tumor organoids that grew in the logarithmic phase, and then cocultured for 24 h at 37°C in the presence of 5% CO_2 with 1:1 mixed medium. The upper chambers were then discarded. Precooled cancer organoid basal medium was used to solubilize the Matrigel encapsulating tumor organoids by repeated pipetting, and the primary tumor cells were retrieved. The suspending matched PBMCs (isolated from the same patients with CRC) prestimulated with 100 ng/mL huIL-15 (Novoprotein, C016) overnight were then cocultured with the retrieved tumor cells at a 20:1 ratio for 4 to 6 h at 37°C in a 5% CO_2 incubator, after which the content of LDH released into the supernatant was measured.

QUANTIFICATION AND STATISTICAL ANALYSIS

All statistical analyses were performed via GraphPad Prism 9.0 software. Each experiment was repeated in triplicate independently. The number of biological replicates and the statistical analysis methods are indicated in each figure legend. The data are expressed as the mean ± standard deviation (SD). A p value less than 0.05 was considered to represent statistical significance.